Beryllium-9 in Cluster Effective Field Theory

Paolo Andreatta
Supervisor: Winfried Leidemann
A thesis presented for the degree of
Doctor of Philosophy

Università degli Studi di Trento
Facoltà di Scienze Matematiche, Fisiche e Naturali
Dipartimento di Fisica

Contents

List of Figures

List of Tables

Chapter 1

Introduction

This thesis makes a contribution to ab initio calculations for light nuclear systems. It belongs to a long term program that aims at calculating observables in quantum composite systems, whose components are groups of distinguishable or indistinguishable particles, which can be bosons and fermions. The spectra of such particle systems can be obtained by diagonalizing the Hamiltonian matrix represented on a suitable basis and by paying attention to a proper convergence. The basis chosen here is the Hyperspherical Harmonics (HH) basis, which ensures the necessary translation and Galilean invariance. Such a basis is more often used for configuration space calculations, however, when working with potentials which are defined in momentum space it can be convenient to diagonalize the Hamiltonian directly in momentum space. In fact my thesis work consists in the development of such a momentum space calculation for an HH basis. In particular, for the proper treatment of S_N symmetries the non-symmetrized hyperspherical harmonics (NSHH) basis and Casimir operator in the Hamiltonian were used.

After having achieved and tested on known results I can then make the initial steps for a calculation of a physical process of astrophysical interest, namely the ^{9}Be photodisintegration, where my contribution consists in the calculation of the ^{9}Be ground state expressed as an assembly of two bosons, the α-particles, and one fermion, the neutron. The interactions needed for such a system is taken from cluster effective field theory, where the α particles and neutrons are considered relevant degrees of freedom.

In order to describe the role of the ^{9}Be photodisintegration, or better its inverse process $\alpha+\alpha+n \rightarrow ^9\text{Be}+\gamma$, for the nucleosynthesis a brief summary of the latter is given in the following.

In the brief span of 20 minutes, according to the Big Bang Nucleosynthesis (BBN) scenario, the lightest elements of our universe, from hydrogen up to lithium, came into being.
In the following hundreds of millions of years the clouds of gas collapsed under gravitational forces and created the first stars and galaxies. It is in these hot furnaces made mainly of hydrogen and helium that the rest of the elements of the Universe were and are still made. This process, called stellar nucleosynthesis, was first proposed in the famous "B^2FH paper" [12] in 1957. Now, more than sixty years from the publication of that article, physicists know that the nucleosynthesis inside the stars is the sum of a number of different processes, and the presence and importance of every one of them is given by the size and age of the star.
Through the p-p chain (for Sun sized or smaller stars) and the CNO cycle (for bigger stars) the hydrogen is burned and becomes helium. After that even the helium undergoes fusion creating carbon and then, if the star is massive enough, this process continues, synthesizing neon, then oxygen, silicon and, in the end, iron. These types of processes stop at this nucleus, ^{56}Fe, since no energy gain through nuclear fusion is possible above this level. If we want to obtain other, heavier nuclei we need to look at other sources. To our knowledge, the mechanisms that allow the creation of these heavy elements are mainly found in two different places: supernovae and asynthotic giant branch (AGB) stars.
In the first case the main engine of heavy nuclei generation is called r-process (rapid neutron capture). In an environment with an high density of neutrons and electrons the nuclei undergo a process of neutron capture, running along the neutron drip line and creating heavy, unstable, neutron-rich nuclei.
In the second case, instead, the neutron capture is slower, allowing β-decays between each capture, making the creation of nuclei go along the so-called line of β-stability.
Among all these nuclei in all these different processes, however, there is one that is quite important, both for its biological role and for being the basis of many processes of nucleosynthesis. That is, carbon.
The usual path for the creation of the ^{12}C nucleus is what is called the triple-α process. However, under the extreme conditions of supernovae, another path becomes dominant, the so called $\alpha\alpha n$ path. Since no stable nucleus with 5 or 8 nucleons exists, the $\alpha\alpha\alpha$ (or, equivalently, triple-α) process allows stars to jump above these gaps and create carbon.
This reaction (also the main source of energy in AGB stars) is composed of two

phases:

$$\alpha + \alpha \rightarrow^{8} Be \tag{1.1}$$

and

$$^{8}Be + \alpha \rightarrow^{12} C + \gamma. \tag{1.2}$$

However, in an high enough abundance of neutrons and alpha particles, another path may dominate over this channel. The first reaction being the same as 1.1, but then it continues as

$$^{8}Be + n \rightarrow^{9} Be + \gamma \tag{1.3}$$

and

$$^{9}Be + \alpha \rightarrow^{12} C + n. \tag{1.4}$$

The $\alpha\alpha n$ channel has been shown to be the predominant path for carbon creation in core-collapse supernovae, meaning that studying the generation of ^{9}Be is of utmost importance for the beginning of the synthesis of heavy nuclei in this environment.
Since ^{8}Be is a resonance just above the continuum threshold of two α particles (at an energy of 91.8 keV above the threshold) for the synthesis of ^{9}Be we can study the following reaction

$$\alpha + \alpha + n \rightarrow^{9} Be + \gamma \tag{1.5}$$

or, equivalently, the inverse one, the photodisintegration of ^{9}Be.
This photodisintegration has been studied in several experiments, the first beginning in the '40s. Various photon sources have been employed in the process, first among them, at quite low resolution, Bremsstrahlung radiation [13, 14] and radioactive isotope measurements [15, 16, 4, 5, 6]. Still, such early experiments where able to restrict to $\sim$2.8 MeV the area where to search. In more recent times, with the improvement of techniques, it has been possible to use more precise laser-induced Compton backscattered γ rays (Utsunomiya *et al.* [3]), investigating the range from 1.78 to 6.11 MeV.
The most recent results used collimated nearly monoenergetic beams (from 1.5 to 5.2 MeV) from free-electron-lasers and ^{3}He-based neutron detectors[1]. These last experiments have shown a much increased cross-section compared to previous results, with important consequences on the models of supernovae nucleosynthesis. All these results are shown in Fig.1.1, where it's also important to notice the threshold energy of a little less than 1.6 MeV, that shows us the

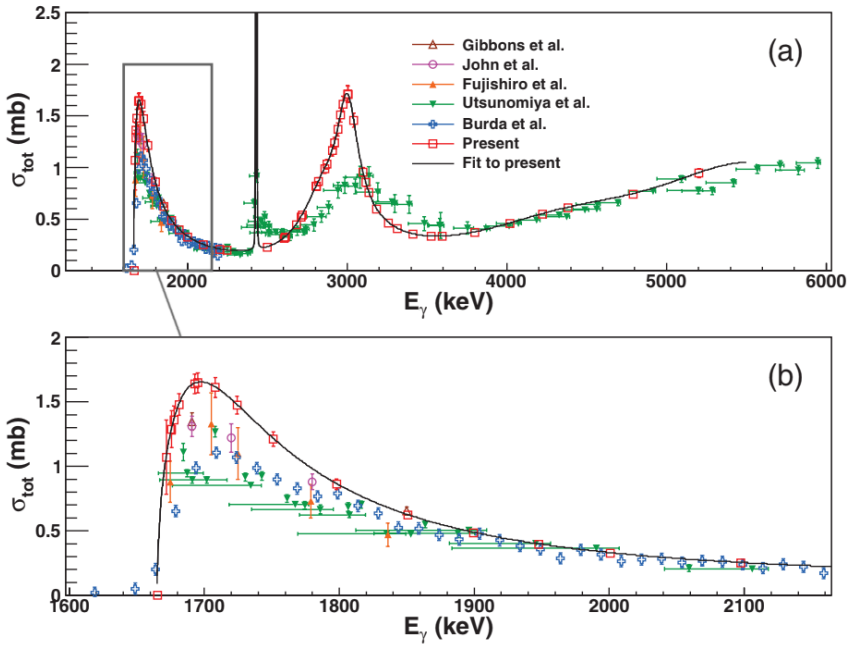

Figure 1.1: Comparison of ^{9}Be photodisintegration cross section from different experiments given in Ref. [1] (data and line labeled with 'present' refer to this). In (a) the shown data is from Burda *et al.* [2] (virtual photons from inelastic electron scattering), Utsunomiya et al. [3] (real photons from inverse Compton scattering), Gibbons [4], John et al. [5] and Fujishiro et al. [6] (real photons from radioisotopes). In (b) an enlargement of the boxed region in (a) is presented.

binding energy between the two α-particles and the neutron products of this reaction.

On the other hand, theoretical calculations for the ^{9}Be photodisintegration can be quite problematic. The configuration of the nucleus and the number of particles involved make calculations with realistic potentials on all nine nucleons of the system extremely expensive in terms of power and time used.

This work is the first step to study such a reaction employing a cluster model instead, that reduces the number of degrees of freedom of the system, simplifying and accelerating the required calculations.

Such an approach is not new for the study of Beryllium-9 photodisintegration. The same technique of clustering was employed by Efros *et al.* in [17], where the ^{9}Be nucleus is described as an $\alpha\alpha n$ system and a calculation for the reaction is achieved by means of phenomenological local potentials. Within the same three-body approach, another calculation of the reaction rate by Casal *et al.* [18] was performed using two-body interactions described by phenomenological potential

models, fitted to $\alpha\alpha$ and αn phase shifts, and a three-body force fixed to reproduce the empirical energies. Both these studies give theoretical predictions in good agreement with the experimental data, however they are both employing phenomenological potential.
In this work instead non-local potentials within Effective Field Theory (EFT), with a more solid theoretical background, have been used. The computationally intensive interaction between nine or more bodies was reduced to a more maneageable interaction between a much smaller number of clusters of nucleons, α particles, and singular neutrons, thanks to the separation of momentum scales present in these nuclei. Using the non-symmetrized hyperspherical harmonics method I have developed a program able to calculate the energy levels of Carbon-12 and Beryllium-9, using this nonlocal, momentum space cluster EFT potential.
The next chapter will introduce the hyperspherical basis and the hyperspherical harmonics functions, showing their properties and how to use them to develop a complete basis of states. The last part will introduce the non-symmetrized basis and the difference with the symmetrized one.
The following chapter will be an introduction to the concept of momentum space, its properties and how to develop an HH basis in this space. It follows an introduction to nonlocal calculations using an HH basis and the benchmark tests for the final program that was generated from the theoretical work laid in the previous parts.
The fourth chapter will introduce the reader to the subject of Effective Field Theory (EFT), to Cluster EFT, and how they were used to generate the interactions used in this program. The results of the calculations and a brief outlook on future prospects will be the subjects of the last two chapters.

Chapter 2

The hyperspherical harmonics (HH) basis

Contents

The first chapter introduced the final objective of this thesis: the creation of a program able to solve the eigenvalue problem for a few-body nuclear system, a program that is able to us both coordinate space and momentum space interactions, local or nonlocal they may be. In particular, the interaction that will be the final suject of study will be a nonlocal, momentum space, EFT potential. But first one must find a suitable basis of functions with which one can build and, consequently, diagonalize the Hamiltonian matrix. Such a basis, as previously mentioned in this thesis, is the non-symmetrized hyperspherical harmonics (NSHH) basis of functions.

2.1 Jacobi coordinates

The first step in order to construct the hyperspherical basis and, subsequently, the HH functions, is given by the Jacobi coordinates.
Through the use of this type of coordinate system we can separate the center of mass (CM) motion from the internal ones in the kinetic term of energy. This is particularly interesting in our case, since it allows us to study specifically only the internal degrees of freedom of our nuclear system.
In a system of A particles, where r_i and m_i are the Cartesian position and the mass of the i-th particle respectively, we introduce the mass-weighted Jacobi coordinates by adopting the so-called reversed order convention:

$$\boldsymbol{\eta}_{A-i} = \sqrt{\frac{m_{i+1}M_i}{mM_{i+1}}}\big(\boldsymbol{r}_{i+1} - \frac{1}{M_i}\sum_{j=1}^{i} m_j \boldsymbol{r}_j\big) \tag{2.1}$$

where $N = A - 1$, $i = 1, .., N$, the constant m is a reference mass (in our case it will be the nucleon mass) and:

$$M_i = \sum_{j=1}^{i} m_j. \tag{2.2}$$

As one can see, the Jacobi coordinates are order-dependent, meaning that changing ordering, coupling and mass parameter one obtains a completely different set of coordinates. Still, it is possible to move, using suitable transformation (that we will show later in the chapter), from one set of Jacobi coordinates to another of different ordering and parameters.
In our case shown above, each $\boldsymbol{\eta}_{A-i}$ vector (for $i > 1$) represents the $(i+1)$-th particle position with respect to the center of mass of the first i particles. In particular the last Jacobi coordinate, $\boldsymbol{\eta}_N$, is directly proportional to the relative distance between the first two particles:

$$\boldsymbol{\eta}_N = \sqrt{\frac{m_1 m_2}{mM_2}}(\boldsymbol{r}_2 - \boldsymbol{r}_1). \tag{2.3}$$

Following the reversed order convention then $\boldsymbol{\eta}_0$ becomes the rescaled CM coordinate:

$$\boldsymbol{\eta}_0 = \sqrt{\frac{M_A}{m}}\boldsymbol{R}_{cm} = \frac{1}{\sqrt{mM_A}}\sum_i m_i \boldsymbol{r}_i. \tag{2.4}$$

We can define the passage between the two bases, Cartesian and Jacobian, using the following matrix S:

$$S = \begin{pmatrix} -\sqrt{\frac{m_2}{m_1 M_2}} & \sqrt{\frac{m_1}{m_2 M_2}} & 0 & \cdots & 0 \\ -\sqrt{\frac{m_3}{M_2 M_3}} & -\sqrt{\frac{m_3}{M_2 M_3}} & \sqrt{\frac{M_2}{m_3 M_3}} & \cdots & 0 \\ -\sqrt{\frac{m_4}{M_3 M_4}} & -\sqrt{\frac{m_4}{M_3 M_4}} & -\sqrt{\frac{m_4}{M_3 M_4}} & \cdots & 0 \\ \vdots & \vdots & \vdots & \ddots & \vdots \\ \sqrt{\frac{1}{M_A}} & \sqrt{\frac{1}{M_A}} & \sqrt{\frac{1}{M_A}} & \cdots & \sqrt{\frac{1}{M_A}} \end{pmatrix} \cdot \mathcal{M} \tag{2.5}$$

where $\mathcal{M}_{ij} = \sqrt{m_i}\delta_{ij}$. Then one can verify the following properties:

$$S^T \cdot S = \mathbb{I} \qquad \det(\mathrm{S}) = 1, \tag{2.6}$$

showing us how S belongs to the $SO(N)$ group. Also, given a vector $\boldsymbol{v}_r$ defined in the Cartesian basis and the same vector $\boldsymbol{v}_\eta$ defined in the Jacobian one, we have the following relation:

$$\boldsymbol{v}_r = \frac{1}{\sqrt{m}} \mathcal{M} \cdot S^T \cdot \boldsymbol{v}_\eta, \tag{2.7}$$

and the relation between volume elements is instead:

$$dV_\eta = \prod_{i=1}^{N} d\boldsymbol{\eta}_i = \prod_{i=1}^{N} \sqrt{\frac{m_i}{m}} d\boldsymbol{r}_i = (\prod_{i=1}^{N} \sqrt{\frac{m_i}{m}}) dV_r. \tag{2.8}$$

From Eq. (2.7) one can then easily convert the Cartesian kinetic operator to the Jacobi version:

$$\begin{aligned} T = -\sum_{i=1}^{A} \frac{\hbar^2}{2m_i} \nabla^2 &= -\frac{\hbar^2}{2} \nabla_r^T \cdot (\mathcal{M}^{-1})^2 \cdot \nabla_r \\ &= -\frac{\hbar^2}{2m} \nabla_\eta^T S \cdot \mathcal{M} \cdot (\mathcal{M}^{-1})^2 \cdot \mathcal{M} \cdot S^T \cdot \nabla_\eta \\ &= -\frac{\hbar^2}{2m} \sum_{i=0}^{N} \nabla_i, \end{aligned} \tag{2.9}$$

where $\nabla_r^T = (\nabla_{r_1}^T, \nabla_{r_2}^T, \cdots)$ and an analogue definition for ∇_η^T.

2.1.1 Permutations and transformations between different sets

As mentioned before, the one chosen above is not the only possible scheme for the Jacobi coordinates. Indeed, one has $A!$ choices of possible Jacobi coordinates, that differ between each other by the sequence of coupling among each of the A

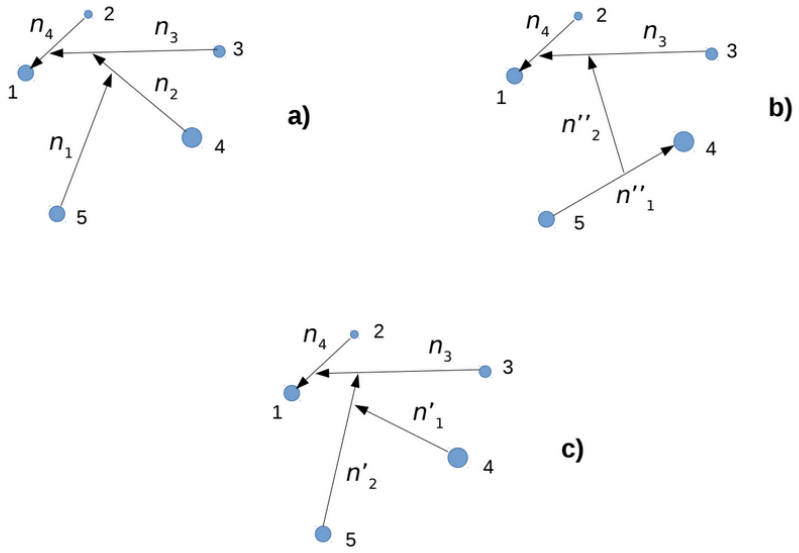

Figure 2.1: Two alternatives to the standard scheme a) of a 5-body Jacobi set of coordinates. In b) a recoupling of particles 4 and 5 is shown: the vector describing their relative positions is connected to the CM of the remaining three particles. In c) the order of coupling of particle 4 and 5 is exchanged with respect to a).

particles composing the system and by the orientation of each $\boldsymbol{\eta}_i$ vector.
All the applications which allow to pass from one scheme to another belong to the group $O(N)$, since they do not involve the relative orientation of the x, y and z components of each $\boldsymbol{\eta}_i$ vector nor the center of mass coordinate. All these applications are compositions of three basic types of transformations, called kinematic rotations: change in sign of a vector, exchange between adjacent particles and recoupling of two particles. In Fig. 2.1 two examples of exchange and recoupling of two particles are shown.
One can generate transformations from one ordering to another through the composition of exchanges between adjacent particles (i and $i+1$) which involve only two coordinates:

$$\begin{pmatrix} \vdots \\ \boldsymbol{\eta}'_{A-i} \\ \boldsymbol{\eta}'_{A-i+1} \\ \vdots \end{pmatrix} = p_{(i,i+1)} \begin{pmatrix} \vdots \\ \boldsymbol{\eta}_{i} \\ \boldsymbol{\eta}_{i+1} \\ \vdots \end{pmatrix} \tag{2.10}$$

where

$$p_{(i,i+1)} \begin{pmatrix} \mathbb{I}_{N-i} & & & \\ & -\cos\beta_i & \sin\beta_i & \\ & \sin\beta_i & \cos\beta_i & \\ & & & \mathbb{I}_{i-2} \end{pmatrix} \tag{2.11}$$

with β_i called the kinematic angle and defined as:

$$\cos^2\beta_i = \frac{m m_{i+1}}{M_i(M_{i-1}+m_{i+1})}. \tag{2.12}$$

However, there is an observation to make. Except the peculiar case of identical masses for every particle a kinematic rotation like the one given in Eq. (2.10) is not equivalent to a spatial permutation. Indeed, a spatial permutation $P_{(i,i+1)}$ between particles i and $i+1$ exchanges, by definition, the r_i and r_{i+1} vectors only:

$$\begin{aligned} P_{(i,i+1)} \cdot \boldsymbol{\eta}[(m_1,r_1),...,(m_i,r_i),(m_{i+1},r_{i+1}),...] \\ = \boldsymbol{\eta}[(m_1,r_1),...,(m_i,r_{i+1}),(m_{i+1},r_i),...] \end{aligned} \tag{2.13}$$

affecting every $\boldsymbol{\eta}_j$ definitions from $j=0$ to $j=A-i$. Kinematic rotations, instead, exchange both masses and positions

$$\begin{aligned} p_{(i,i+1)} \cdot \boldsymbol{\eta}[(m_1,r_1),...,(m_i,r_i),(m_{i+1},r_{i+1}),...] \\ = \boldsymbol{\eta}[(m_1,r_1),...,(m_{i+1},r_{i+1}),(m_i,r_i),...] \end{aligned} \tag{2.14}$$

and end up affecting only the definitions of $\boldsymbol{\eta}_i$ and $\boldsymbol{\eta}_{i+1}$.
Still, we can find a link between the two by introducing another type of transformation, the transformations between two different sets of mass parameters. Given one set of masses, ζ, with

$$\zeta = \{m_i > 0; i = 1,...A\} \tag{2.15}$$

in which a set of Jacobi coordinates $\boldsymbol{\eta}_i^{\zeta}$ is defined, it is possible to operate a transformation from this set to another set of masses (and relative set of Jacobi coordinates) ζ'. This is accomplished through the use of the matrix of this transformation, $W_{\zeta\zeta'}$, that can be built from the particular case where the only different mass between the two sets is in the A-th particle. Then it is easy to see that

$$\eta_i^{\zeta} = \begin{cases} a_A \eta_i^{\zeta'} & i=1 \\ \eta_i^{\zeta'} & i=2,...,N \end{cases} \tag{2.16}$$

with

$$a_A = \sqrt{\frac{m_A M'_A}{m'_A M_A}} \qquad M'_A = M_A - m_A + m'_A, \tag{2.17}$$

making $W_{\zeta\zeta'} = W_{(A)}$ assume the simple form of

$$W_{(A)} = \begin{pmatrix} a_A & \\ & \mathbb{I}_{N-1} \end{pmatrix}. \tag{2.18}$$

Then if the mass to change is located in the generic i-th position, one can always apply a sequence of kinematical rotations in order to move the (m_i, r_i) couple in the last coupling position, and then come back after the application of the scaling transformation $W_{(A)}$:

$$W_{(i)} = \Big[\prod_{\alpha=N}^{i} p^{\zeta'}_{\alpha,\alpha+1} \Big] W_{(A)} \Big[\prod_{\alpha=i}^{N} p^{\zeta}_{\alpha,\alpha+1} \Big] \tag{2.19}$$

where $p^{\zeta'}_{\alpha,\alpha+1}$ is the kinematical rotation in ζ', $p^{\zeta}_{\alpha,\alpha+1}$ in ζ.
$W_{\zeta\zeta'}$ is then constructed as

$$W_{\zeta\zeta'} = \prod_{i=1}^{A} W_{(i)}. \tag{2.20}$$

With this new transformation we can finally find the link between spatial permutations and kinematical rotations in the Jacobi coordinates:

$$\begin{aligned} P_{ij}\boldsymbol{\eta} &= W_{ij} \cdot p_{i,j}\boldsymbol{\eta}[(m_1, r_1), ..., (m_i, r_i), ..., (m_j, r_j), ...] = \\ &= W_{ij} \cdot \boldsymbol{\eta}[(m_1, r_1), ..., (m_j, r_j), ..., (m_i, r_i), ...] = \qquad (2.21) \\ &= \boldsymbol{\eta}[(m_1, r_1), ..., (m_i, r_j), ..., (m_j, r_i), ...] \qquad (2.22) \end{aligned}$$

2.2 Hyperspherical coordinates[1]

After generating a set of Jacobi basis the next step we need to take is to express every single vector $\boldsymbol{\eta_k}$ in spherical coordinates. So, for every $\boldsymbol{\eta_k}$ we will have one radial coordinate η_k and two angular coordinates $\hat{\eta}_k = (\theta_k, \varphi_k)$.
The final step we need to do in order to construct the hyperspherical basis is to take the N radial coordinates and transform them in $N-1$ angular coordinates and a single hyperradial coordinate ρ. To better comprehend how it's done we should start from the case of two Jacobi radial coordinates, η_1 and η_2. We

[1] This section and the following ones are liberally inspired by the doctoral work of Nir Barnea[19]

can parameterize them using the hyperradial coordinate ρ_2 and the hyperradial angle Φ_2, in polar coordinates:

$$\begin{cases} \eta_1 = \rho_2 \cos\Phi_2 \\ \eta_2 = \rho_2 \sin\Phi_2 \end{cases} \tag{2.23}$$

Adding another angle and with a different hyperradius ρ_3 we can describe three Jacobi radial coordinates using spherical coordinates:

$$\begin{cases} \eta_1 = \rho_3 \cos\Phi_3 \cos\Phi_2 \\ \eta_2 = \rho_3 \cos\Phi_3 \sin\Phi_2 \\ \eta_3 = \rho_3 \sin\Phi_3 \end{cases} \tag{2.24}$$

And we can add up to $N-1$ angles, in order to describe N radial η_i:

$$\begin{cases} \eta_1 = \rho_N \cos\Phi_N ... \cos\Phi_3 \cos\Phi_2 \\ \eta_2 = \rho_N \cos\Phi_N ... \cos\Phi_3 \sin\Phi_2 \\ \vdots \\ \eta_i == \rho_N \cos\Phi_N ... \cos\Phi_{i+1} \sin\Phi_i \\ \vdots \\ \eta_{N-1} = \rho_N \cos\Phi_N \sin\Phi_{N-1} \\ \eta_N = \rho_N \sin\Phi_N \end{cases} . \tag{2.25}$$

In conclusion, we can describe N different radial coordinates using a S^{N-1} hypersphere in $\mathbb{R}^N$. We can reverse the previous definition and define the hyperradius ρ and every single hyperangle Φ_i with the radial Jacobi coordinates:

$$\begin{cases} \sin\Phi_n = \eta_n/\rho_n \\ \cos\Phi_n = \rho_{n-1}/\rho_n \end{cases} \Rightarrow \begin{cases} \rho_n^2 = \rho_{n-1}^2 + \eta_n^2 = \sum_{j=1}^{n} \eta_j^2 \\ \sin\Phi_i = \frac{\eta_i}{\sqrt{\eta_1^2+...+\eta_i^2}} \end{cases} . \tag{2.26}$$

To note that the hyperradial coordinate $\rho = \rho_N$ is symmetric with respect to permutations of the particles.

With these formulae then the $3N = 3(A-1)$ internal coordinates for an A-particle system can be represented by an hyperradial coordinate ρ and $3N - 1 = 3A - 4$ hyperangular coordinates $\Omega_{(N)} = \{\hat{\eta}_1, \hat{\eta}_2, \cdots, \hat{\eta}_N, \Phi_2, \cdots, \Phi_N\} = \{\Omega_1, \Omega_2, \cdots, \Omega_N, \Phi_2, \cdots, \Phi_N\}$, with the hyperangles Φ_n varying in the range $\frac{\pi}{2} \geq \Phi_N \geq 0$. In short, we have developed the following parametrization:

$$\boldsymbol{\eta}(\rho, \Omega_{(N)}) : \mathbb{R}^{3N} \to \mathbb{R}_+ \times S_+^{N-1} \times (S^2)^N. \tag{2.27}$$

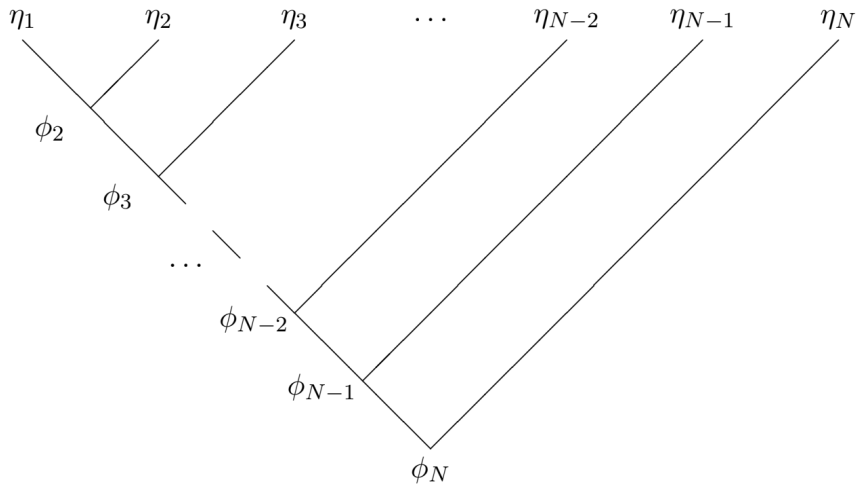

Figure 2.2: Tree diagram representing the standard scheme of hyperangular coordinates. The explicit relations are shown in Eq. (2.25)

We can then define the hyperradial volume element (with $\rho = \rho_N$) as:

$$\begin{aligned} dV_{3N} &= \rho^{3N-1} d\rho dS_{3N-1} = \\ &= \rho^{3N-1} d\rho \sin^2(\Phi_N) \cos^{3N-4} \Phi_N d\Phi_N d\Omega_N dS_{3N-4} = \\ &= \rho^{3N-1} d\rho \sin\theta_1 d\theta_1 d\varphi_1 \prod_{i=2}^{N} \sin\theta_i d\theta_i d\varphi_i (\sin\Phi_i)^2 (\cos\Phi_i)^{3i-4} d\Phi_i \end{aligned} \tag{2.28}$$

where dS_{3N-1} is the volume element associated with the $3N-1$ dimensional hypersphere and $d\Omega_N$ is the volume associated with the angular part of the Nth Jacobi coordinate η_N. Like for the Jacobi coordinates also in the hyperspherical case we can choose between several different sets of coordinates. A powerful tool in representing the variety of such sets is given by the tree diagram, first introduced by N. Ya. Vilenkin et al. in [20]. In Fig. 2.2 the set of Eq. (2.25) is schematized.

Each hyperangle Φ_i is related to the i-th node: if the segment joining this node with the upper one extends to the right, a factor equal to $\sin\Phi_i$ is associated, otherwise $\cos\Phi_i$. Each η_i is obtained by the product of ρ with each sine or cosine factor associated to each node starting from the lowest vertex and following the track to the η_i termination.

2.2.1 The Laplace operator in hyperspherical coordinates

The hyperspherical coordinates are a generalization of the spherical coordinates for a A-body system, the hyperspherical harmonics functions a generalization

of the spherical harmonics functions. These are eigenfunctions of the angular momentum operator, contained in the relative kinetic energy operator so, in order to generate the HH, we need to search for a generalization of the Laplace operator.

The internal kinetic energy operator for a two particle system is given by the three dimensional laplacian, that we express in terms of the relative motion Jacobi coordinate η_1 and the corresponding angular coordinates Ω_1

$$\Delta_{(1)} = \Delta\boldsymbol{\eta}_1 = \Delta_{\eta_1} - \frac{1}{\eta_1^2}\hat{l}_1^2 \tag{2.29}$$

where the radial part is given by

$$\Delta_{\eta_1} = \frac{\partial^2}{\partial\eta_1^2} + \frac{2}{\eta_1^2}\frac{\partial}{\partial\eta_1} \tag{2.30}$$

and $\hat{l}_1$ is the angular momentum operator of the relative motion.

If we go to the three particle system we can describe the internal kinetic energy with a six dimensional Laplace operator which is a sum of the three dimensional Laplace operators that act separately on coordinates η_1 and η_2.

$$\Delta_{(2)} = \Delta\boldsymbol{\eta}_1 + \Delta\boldsymbol{\eta}_2 = \Delta_{\eta_1} + \Delta_{\eta_2} - \frac{1}{\eta_1^2}\hat{l}_1^2 - \frac{1}{\eta_2^2}\hat{l}_2^2 \tag{2.31}$$

Using equation (2.23) we can transform the Jacobi coordinates η_1 and η_2 in the hyperradial coordinate ρ_2 and the hyperangle Φ_2, obtaining

$$\Delta_{(2)} = \Delta_{\rho_2} - \frac{1}{\rho_2^2}\hat{K}_2^2. \tag{2.32}$$

The radial part of the this equation depends only on the hyperradius ρ_2

$$\Delta_{\rho_2} = \frac{\partial^2}{\partial\rho_2^2} + \frac{5}{\rho_2^2}\frac{\partial}{\partial\rho_2}. \tag{2.33}$$

The hyperspherical angular momentum operator $\hat{K}_2^2$ is instead expressed in terms of the hyperangle Φ_2 and the two "classical" angular momentum operators l_1^2 and l_2^2 as follows

$$\hat{K}_2^2 = -\frac{\partial^2}{\partial\Phi_2^2} - 4\cot(2\Phi_2)\frac{\partial}{\partial\Phi_2} + \frac{1}{\cos^2\Phi_2}\hat{l}_1^2 + \frac{1}{\sin^2\Phi_2}\hat{l}_2^2 \tag{2.34}$$

The internal total angular momentum of the system is $\hat{L}_2 = \hat{l}_1 + \hat{l}_2$. Note that $\hat{L}_2^2$ and $\hat{L}_{2_z}$ commute with $\Delta_{(2)}$, $\hat{l}_1^2$, $\hat{l}_2^2$ and $\hat{K}_2^2$.

From these examples is then easy to find the generalization to the $3N$ dimensional Laplace operator, that describes the internal kinetic energy of the $N+1$ particle system. The laplacian will be a sum over all the three dimensional

Laplace operator that act on the Jacobi coordinates $\eta_1, \eta_2, \cdots, \eta_N$

$$\Delta_{(N)} = \sum_{i=1}^{N} \Delta_{\boldsymbol{\eta}_i} = \sum_{i=1}^{N} \left(\Delta_{\eta_i} - \frac{1}{\eta_i^2} \hat{l}_i^2 \right). \tag{2.35}$$

We can express it also using a recurrence relation

$$\Delta_{(N)} = \Delta_{(N-1)} + \Delta_{\boldsymbol{\eta}_N} = \Delta_{\rho_{N-1}} + \Delta_{\eta_N} - \frac{1}{\rho_{N-1}^2} \hat{K}_{N-1}^2 - \frac{1}{\eta_N^2} \hat{l}_N^2. \tag{2.36}$$

Then we can apply Eq. (2.26), transforming the coordinates ρ_{N-1} and η_N into the hyperradius $\rho = \rho_N$ and the hyperangle Φ_N. This will result in

$$\Delta_{(N)} = \Delta_{\rho_N} - \frac{1}{\rho_N^2} \hat{K}_N^2 \tag{2.37}$$

where the (hyper)radial part is

$$\Delta_{\rho_N} = \frac{\partial^2}{\partial \rho_N^2} + \frac{3N-1}{\rho_N^2} \frac{\partial}{\partial \rho_N} = \frac{1}{\rho_N^{3N-1}} \frac{\partial}{\partial \rho_N} \rho_N^{3N-1} \frac{\partial}{\partial \rho_N}. \tag{2.38}$$

The hyperspherical or grand angular momentum operator $\hat{K}_n^2$, $n = 2, ..., N$, can then be expressed in terms of the squared angular momentum associated to the nth Jacobi coordinate, $\hat{l}_n^2$ and $\hat{K}_{n-1}^2$, as follows:

$$\hat{K}_n^2 = -\frac{\partial^2}{\partial \phi_n^2} - \frac{3n-6-(3n-2)\cos(2\phi_n)}{\sin(2\phi_n)} \frac{\partial}{\partial \phi_n} + \frac{1}{\cos^2 \phi_n} \hat{K}_{n-1}^2 + \frac{1}{\sin^2 \phi_n} \hat{l}_n^2 \tag{2.39}$$

where we define $\hat{K}_1^2 = \hat{l}_1^2$ and the internal n particle angular momentum operator as $\hat{L}_n = \hat{L}_{n-1} + \hat{l}_n$. The operators $\hat{l}_n^2$, $\hat{K}_n^2$, $\hat{K}_{n-1}^2$, $\hat{L}_n^2$ and $\hat{L}_{n_z}$ then commute with each other thus giving us the possibility of labelling each hyperspherical state with a complete set of quantum numbers $K_N^2, K_{N-1}^2, \cdots, K_2^2$ corresponding to the hyperspherical angular momentum, $L_N, L_{N-1}, \cdots, L_2, M_{N_z}$ corresponding to the spatial angular momentum and $l_N, l_{N-1}, \cdots, l_2, l_1$ for the angular part of the Jacobi coordinates.

2.3 Hyperspherical harmonics functions

The angular part of the internal state for two particle is described by the spherical harmonic $Y_{l_1,m_1}(\Omega_1)$. Adding a third particle and taking the state $Y_{l_2,m_2}(\Omega_2)$ we can form the three particle state $\phi_{L_2 M_2; l_1 l_2}(\Omega_2)$, eigenstate of the operators $\hat{l}_1^2$, $\hat{l}_2^2$, $\hat{L}_2^2$ and $\hat{M}_{2_z}$. This three particle state is obtained by coupling the states $Y_{l_1,m_1}(\Omega_1)$ and $Y_{l_2,m_2}(\Omega_2)$ with the use of Clebsch-Gordan coefficients:

$$\phi_{L_2 M_2; l_1 l_2}(\Omega_1, \Omega_2) = \sum_{m_1 m_2} (l_1 m_1 l_2 m_2 | L_2 M_2) Y_{l_1,m_1}(\Omega_1) Y_{l_2,m_2}(\Omega_2). \tag{2.40}$$

The next step in the construction of the HH for three particle systems is given by the definition of the eigenfunctions Ψ of $\hat{K}_2^2$ (2.34). They are functions of the hyperangle Φ_2, dependent on the quantum numbers K_2, l_2 and $K_1(\equiv l_1)$ as follows:

$$\Psi_{K_2;l_2l_1}(\Phi_2) = \mathcal{N}_2(K_2;l_2l_1)(\sin\Phi_2)^{l_2}(\cos\Phi_2)^{l_1}P_{n_2}^{(l_2+\frac{1}{2},l_1+\frac{1}{2})}(\cos 2\Phi_2) \quad (2.41)$$

where $P_{n_2}^{(l_2+\frac{1}{2},l_1+\frac{1}{2})}$ is the Jacobi polynomial, n_2 is a non negative integer and

$$K_2 = 2n_2 + l_1 + l_2. \quad (2.42)$$

The normalization constant is

$$\mathcal{N}_2(K_2;l_2l_1) = \left[\frac{(2K_2+4)n_2!\Gamma(n_2+l_2+l_1+2)}{\Gamma(n_2+l_2+\frac{3}{2})\Gamma(n_2+l_1+\frac{3}{2})}\right]^{\frac{1}{2}} \quad (2.43)$$

and the eigenvalues of the $\hat{K}_2^2$ corresponding to this functions are $K_2(K_2+4)$, where $K_2 \geq l_1 + l_2 \geq L_2 \geq 0$. The parity is the same of $l_1 + l_2$.
The hyperspherical function for three particles, eigenfunction of $\hat{K}_2^2$ and $\hat{L}_2$, is obtained simply multiplying Ψ and ϕ:

$$\mathcal{Y}_{[K_2]}(\Omega_{(2)}) = \Psi_{K_2;l_2l_1}(\Phi_2)\phi_{L_2M_2;l_1l_2}(\Omega_1,\Omega_2,\Phi_2), \quad (2.44)$$

with $\Omega_{(2)} = \{\Omega_1,\Omega_2\}$.
This state is dependent on five quantum numbers, K_2, L_2, M_2, l_1 and l_2, here grouped under the symbol $[K_2]$, since it is dependent by five coordinates ($\Omega_1 = (\theta_1,\varphi_1)$, $\Omega_2 = (\theta_2,\varphi_2)$ and Φ_2 aggregated under $\Omega_{(2)}$.)
Since $K_1 = l_1$ it is not possible to extract the generic characteristics of the recursive construction of the hyperspherical functions in general. We therefore need to describe the four particle case.
First we need to couple the two-body HH in Eq.(2.44) with the function $Y_{l_3,m_3}(\Omega_3)$. This is done, as in the previous case, with the aid of the Clebsch-Gordan coefficients:

$$\phi_{L_3M_3;[K_2]l_3}(\Omega_{(2)},\Omega_3) = \sum_{M_2m_3}(L_2M_2l_3m_3|L_3M_3)\mathcal{Y}_{[K_2]}(\Omega_{(2)})Y_{l_3,m_3}(\Omega_3). \quad (2.45)$$

Using Eq. (2.24) it is then possible to generate the eigenfunctions of the operator $\hat{K}_3^2$ in a manner similar to the previous one:

$$\Psi_{K_3;l_3K_2}(\Phi_3) = \mathcal{N}_2(K_3;l_3K_2)(\sin\Phi_3)^{l_3}(\cos\Phi_3)^{K_2}P_{n_3}^{(l_3+\frac{1}{2},K_2+2)}(\cos(2\Phi_3)) \quad (2.46)$$

with

$$K_3 = 2n_3 + K_2 + l_3. \quad (2.47)$$

and

$$\mathcal{N}_2(K_3; l_3 K_2) = \left[\frac{(2K_3+7)n_3!\Gamma(n_3+l_3+K_2+\frac{7}{2})}{\Gamma(n_3+l_3+\frac{3}{2})\Gamma(n_3+K_2+3)}\right]^{\frac{1}{2}}. \tag{2.48}$$

The eigenvalues of $\hat{K}_3^2$ corresponding to these eigenfunctions are $K_3(K_3+7)$, with $K_3 \geq K_2 + l_3 \geq 0$ and the same parity of $K_2 + l_3$.
In a manner akin to the previous, we construct the HH

$$\mathcal{Y}_{[K_3]}(\Omega_{(3)}) = \Psi_{K_3;l_3K_2}(\Phi_3)\phi_{L_3M_3;[K_2]l_3}(\Omega_{(2)}, \Omega_3), \tag{2.49}$$

where $[K_3]$ stands for $K_3, L_3, M_3, K_2, L_2, l_3$ and $\Omega_{(3)} = \{\Omega_1, \Omega_2, \Omega_3, \Phi_2, \Phi_3\} = \{\Omega_{(2)}, \Omega_3, \Phi_3\}$.
From these examples it is now possible to deduce how to obtain the N+1 particle hyperspherical function $\mathcal{Y}_{[K_N]}$. First one needs to couple the N particle HH $\mathcal{Y}_{[K_{N-1}]}$ and the spherical harmonic $Y_{l_N,m_N}(\Omega_N)$ using Clebsch-Gordan coefficients:

$$\begin{aligned}&\phi_{L_N M_3 N;[K_{N-1}]l_N}(\Omega_{(N-1)}, \Omega_N) = \\ &= \sum_{M_{N-1}m_N} (L_{N-1}M_{N-1}l_N m_N | L_N M_N)\mathcal{Y}_{[K_{N-1}]}(\Omega_{(N-1)})Y_{l_N,m_N}(\Omega_N).\end{aligned} \tag{2.50}$$

Second, one constructs the orthonormalized eigenfunctions of the grand angular momentum operator $\hat{K}_N^2$

$$\begin{aligned}\Psi_{K_N;l_N K_{N-1}}(\Phi_N) = \mathcal{N}_N(K_N; l_N K_{N-1})(\sin\Phi_N)^{l_N}(\cos\Phi_N)^{K_N} \times \\ \times P_{n_N}^{(l_N+\frac{1}{2}, K_{N-1}+\frac{3N-5}{2})}(\cos 2(\Phi_N))\end{aligned} \tag{2.51}$$

with

$$K_N = 2n_N + K_{N-1} + l_N. \tag{2.52}$$

and

$$\mathcal{N}_N(K_N; l_N K_{N-1}) = \left[\frac{(2K_N+3N-2)n_N!\Gamma(n_N+l_N+K_{N-1}+\frac{3N-2}{2})}{\Gamma(n_N+l_N+\frac{3}{2})\Gamma(n_N+K_{N-1}+\frac{3N-5}{2})}\right]^{\frac{1}{2}}. \tag{2.53}$$

The eigenvalues of the operator $\hat{K}_N^2$ for the functions $\Psi_{K_N;l_N K_{N-1}}$ are $K_N(K_N+3N-2)$, where $K_N \geq K_{N-1} + l_N \geq 0$ and has the same parity as $K_{N-1} + l_N$. As the last step we construct $\mathcal{Y}_{[K_N]}$, N (Jacobi) coordinates, $N+1$ particle functions, coupled to a total angular momentum L_N. As usual the method is composed of simply the product of Ψ and ϕ,

$$\mathcal{Y}_{[K_N]}(\Omega_{(N)}) = \Psi_{K_N;l_N K_{N-1}}(\Phi_N)\phi_{L_N M_3 N;[K_{N-1}]l_N}(\Omega_{(N-1)}, \Omega_N), \tag{2.54}$$

where $[K_N]$ stands for $K_N, L_N, M_N, K_{N-1}, L_{N-1}, l_N$ and $\Omega_{(N)} = \{\Omega_{(N-1)}, \Omega_N, \Phi_{N-1}\}$. This means that the A-body HH function can be expressed in the following form:

$$\mathcal{Y}_{[K_N]}(\Omega_{(N)}) = [Y_{l_1}(\hat{\boldsymbol{\eta}}_1) \otimes Y_{l_2}(\hat{\boldsymbol{\eta}}_2)|_{L_2} \otimes ... \otimes Y_{l_{N-1}}(\hat{\boldsymbol{\eta}}_{N-1})|_{L_{N-1}} \times \times Y_{l_N}(\hat{\boldsymbol{\eta}}_N)|_{L_N M_N}] \Big[\prod_{i=2}^{N} \Psi_{K_i; l_i K_{i-1}}(\Phi_i)\Big] \tag{2.55}$$

2.4 Complete HH basis

While the HH functions are a powerful tool, they're not enough to generate a complete basis of functions of our space. Not only we are still missing the hyperradial part but also the spin and isospin one. Indeed, a function of a basis in this space will be of the form

$$|\Phi_i\rangle = \left|\mathcal{R}_{r_i}\mathcal{Y}_{[K_N]_i}\right\rangle \otimes \left|\chi_{[S_A]_i}\chi_{[T_A]_i}\right\rangle \tag{2.56}$$

where $\mathcal{R}_{r_i}$ are the hyperradial functions, $\chi_{[S_A]_i}$ and $\chi_{[T_A]_i}$ are the spin and isospin states.

The hyperradial basis is generated from a set of generalized Laguerre polynomials $L_n^{(\nu)}(\rho/\beta)$ coupled with the appropriate weights

$$\mathcal{L}_n(\rho) = \sqrt{\frac{n!}{(n+\nu)!}} L_n^{(\nu)}(\rho/\beta) e^{-\frac{\rho}{2\beta}} \left(\frac{\rho}{\beta}\right)^{\frac{\nu-3A+4}{2}} \tag{2.57}$$

where β is a variational parameter with dimension of a length, that has been studied in order to analyze the convergence of bound state, and n is an integer number $0 < n < n_{max}$.

By using the properties of the Laguerre polynomials we can calculate the following integral in an analytical way

$$\begin{aligned} R_{n,n'}^{\nu;a} &= \langle \mathcal{L}_n(r)| \, r^a \, |\mathcal{L}_{n'}(r)\rangle = \\ &= \sqrt{\frac{n!n'!}{(n+\nu)!(n'+\nu)!}} \int_0^\infty e^{-r} r^\nu L_n(r) \mathcal{L}_{n'}(r) r^a = \\ &= \sqrt{\frac{n!(n+\nu)!}{n'!(n'+\nu)!}} \sum_{m=0}^{n} (-1)^m \frac{(\nu+a+m)!(-a-m)_{n'}}{(n-m)!(\nu+m)!m!}, \end{aligned} \tag{2.58}$$

meaning that we can analytically evaluate the kinetic radial matrix elements:

$$\langle \mathcal{L}_n(r)| \, \nabla_\rho \, |\mathcal{L}_{n'}(r)\rangle = \frac{1}{4}\delta_{nn'} - \frac{3N-1+2n'}{2} R_{n,n'}^{\nu;-1} + (3N-\nu+2)\times \times \left[n' R_{n,n'}^{\nu;-2} - \sqrt{n'(n'+\nu)} R_{n,n'-1}^{\nu;-1}\right]. \tag{2.59}$$

Choosing $\nu = 3N-1$ we can recover the volume element dV_ρ defined in Eq.

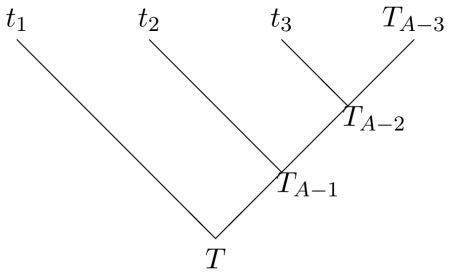

Figure 2.3: Tree diagram representing the sequential reversed-order A-body isospin coupling.

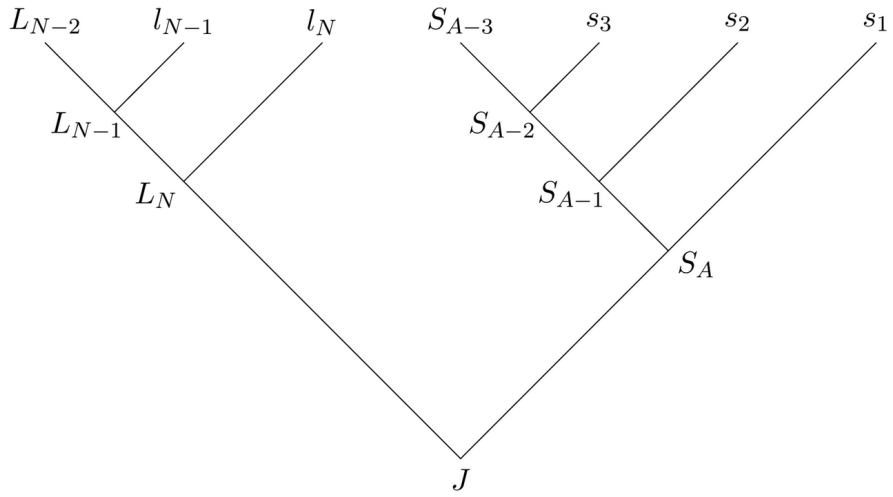

Figure 2.4: Tree diagram representing the coupling scheme between the orbital angular momentum L_N and the total spin S_A in a A-body non-central basis.

(2.28), making this the most natural choice.

The spin and the isospin basis were both defined on a reversed sequential coupling. By denoting as s_i and t_i, respectively, the spin and the isospin quantum numbers of the i-th particle, each spin and isospin state can be identified by the following notation:

$$[S_A] = s_A, s_{A-1}, ..., s_1; S_2, ..., S_{A-1}, S_A \tag{2.60}$$

$$[T_A] = t_A, t_{A-1}, ..., t_1; T_2, ..., T_{A-1}, T_A; T_{A_z}; \tag{2.61}$$

where S_i is the total spin quantum number of the system composed by particles from A to $A - i + 1$ (the same notation is used for the isospin part). T_{A_z} is the projection on the z axis of the total isospin T_A. As seen in Fig. 2.3, the isospin coupling scheme can be represented in the tree diagram form.

In the case of a central force L_N and S_N are conserved, meaning that they

are good quantum numbers for defining the eigenstates of $\hat{H}$ ($[K_N; S_N]_c = [K_N] \otimes [S_A]$). In the non-central case however S_N and L_N are not good quantum numbers anymore, and only the total angular momentum J, together with the isospin numbers T_A and T_{A_z}, can be used to define the angular plus spin/isospin wavefunction ($[K_N; S_N]_c = [K_N; S_{A-2}; [[L_{N-1}, l_N]_{L_N}; [S_{A-1}, s_A]_{S_A}]_J]$), leading to a much bigger basis (Fig. 2.4).

2.5 The Symmetrized and the Non-Symmetrized HH Basis

The HH functions do not possess any intrinsic, particular symmetry under particle permutations, then they have to be manually symmetrized.
One approach consists in a recursive construction of HH functions by realizing irreducible representations not only of the orthogonal group $O(3N)$ but also of the group $O(N)$, accordingly to the chain $O(3N) \subset O(3) \otimes O(N)$:

$$\begin{array}{ccccccccccc} O(3N-3) \supset O(3) \otimes & O(N-1) & \supset & O(N-2) & \cdots & \supset & O(2) & & \\ & \cup & & \cup & & & \cup & & \\ & S_N & \supset & S_{N-1} & \cdots & \supset & S_3 & \supset & S_2 \end{array} \tag{2.62}$$

Such an approach has been developed through an efficient technique by N. Barnea more than two decades ago [19] and it led to the first 6-body calculation through the use of the HH method [21]. Up to 7-body calculations have also been performed, but limited to central potentials.
This approach for a few-body system of fermions is quite powerful, since with an antisymmetric wavefunction Ψ_A one can calculate all the matrix elements for a potential by calculating only the matrix element of one pair of particles

$$\langle \Psi_A | \sum_{i<j} V_{ij} | \Psi_A \rangle = \frac{N(N-1)}{2} \langle \Psi_A | V_{12} | \Psi_A \rangle . \tag{2.63}$$

However, the couples analyzed in this program (nn, $\alpha\alpha$ and αn) have all different symmetries, making the implementation of this method exceedingly difficult.
An alternative HH approach to the few-body problem has been developed a few years ago by M. Gattobigio et al. in ref. [22] and it is based on the use of the Hyperspherical Harmonics basis without previous symmetrization.
The eigenvectors of the A-body Hamiltonian possess a well defined symmetry under particle permutations, and this symmetry can be identified by means of the application of the Casimir operator of the group of permutations of A objects, $C(A)$. When the spatial part of the eigenstates is found and its symmetry

determined, the spin and isospin parts are combined in order to obtain the desired total permutational symmetry.
A variation on the non-symmetrized HH (NSHH) approach has been later introduced by N. Barnea et al. and it is based on the definition of a pseudoHamiltonian as a suitable combination of the A-body Hamiltonian and the $C(A)$ operator. The lowest eigenvectors of such an operator possess the desired permutational symmetry and they can be calculated by means of fast diagonalization procedures, in this case the Lanczos procedure, given its property of fast convergence on the lowest eigenstates, was chosen.
In order to tackle the problem of having to calculate the matrix elements for all the couples of particle ij, since we are missing an intrinsic symmetry of the wavefunction, we use permutation matrices in a similar manner to Eq:(2.22):

$$\langle \Psi_{NSHH} | V_{ij} | \Psi_{NSHH} \rangle = \langle \Psi_{NSHH} | P_{1i}^{-1} P_{2j}^{-1} V_{12} P_{1i} P_{2j} | \Psi_{NSHH} \rangle . \tag{2.64}$$

with

$$P_{ab} = \prod_{s=a}^{b-1} \mathcal{P}^{(s)} \prod_{s=b-2}^{a} \mathcal{P}^{(s)}, \quad a < b. \tag{2.65}$$

The unitary matrix $\mathcal{P}^{(j)}$ is defined as

$$\mathcal{P}^{(j)}_{[K_N][K'_N]} = \int \mathcal{Y}_{*[K_N]}(\Omega_N) \mathcal{Y}_{[K'_N]}(\Omega_N^{(j)}) d\Omega_N \tag{2.66}$$

and represents the kinematic rotation between the two mass-position pairs (m_j, r_j) and (m_{j+1}, r_{j+1}) in the HH basis.
It can be shown (see [23]) to be equal to

$$\begin{aligned} \mathcal{P}^{(j)}_{[K_N][K'_N]} = & \left[\prod_{\alpha=1}^{i-2} \delta_{l_\alpha, l'_\alpha} \prod_{k=2}^{i-2} \delta_{L_k, L'_k} \delta_{K_k, K'_k} \right]^{(i)} \mathcal{B}^{L_{i-2} K_{i-2} L_i K_i}_{l_{i-1} l'_{i-1} L_{i-1} L'_{i-1} K'_{i-1}} \\ & \cdot \left[\prod_{\alpha=i+1}^{N} \delta_{l_\alpha, l'_\alpha} \prod_{k=i+1}^{N} \delta_{L_k, L'_k} \delta_{K_k, K'_k} \right]. \end{aligned} \tag{2.67}$$

The $\mathcal{B}$ matrices represent the blocks of the $\mathcal{P}$ matrix and are combinations recouplings by means of the Tree, the T and the Raynal-Revai coefficients:

$$\begin{aligned} {}^{(i)}\mathcal{B}^{L_{i-2} K_{i-2} L_i K_i}_{l_{i-1} l'_{i-1} L_{i-1} L'_{i-1} K'_{i-1}} = & \sum_{L_{i,i-1}} T^{L_{i-2} l_{i-1} l_i}_{L_{i-1}, L_{i,i-1}, L_i} T^{L_{i-2} l'_{i-1} l'_i}_{L_{i-1}, L_{i,i-1}, L_i} \cdot \\ & \cdot \sum_{K_{i-1,i}} T^{\alpha_{K_{i-1}} \alpha_{l_{i-1}} \alpha_{l_i}}_{K_{i-1} K i, i-1 K_i} T^{\alpha_{K_{i-1}} \alpha'_{l_{i-1}} \alpha'_{l_i}}_{K_{i-1} K i, i-1 K_i} \cdot \mathcal{R}^{K_{i,i-1}, L_{i,i-1}}_{l_{i-1} l_i, l'_{i-1} l'_i}, \end{aligned} \tag{2.68}$$

with

$$T^{L_{i-2}l_{i-1}l_i}_{L_{i-1},L_{i,i-1},L_i} = (-1)^{L_{i-2}+l_{i-1}+l_i+L_i}\sqrt{2L_{i-1}+1}\cdot \cdot\sqrt{2L_{i,i-1}+1}\begin{Bmatrix} L_{i-2} & l_{i-1} & l_i \\ l_i & L_i & L_{i,i-1} \end{Bmatrix}, \tag{2.69}$$

and $\mathcal{R}^{K_{i,i-1},L_{i,i-1}}_{l_{i-1}l_i,l'_{i-1}l'_i}(\beta_j)$ the Raynal-Revai coefficients as described in [24].
Even without a symmetrized basis one can then calculate all the potential matrix elements through the use of permutation matrices and the Casimir operator. This last approach is the one adopted by the present work. Here I just stress that the avoidance of the symmetrization procedure, however, is partly counterweighted by the larger dimension of the basis, which is not anymore constrained by the permutational symmetry.

Chapter 3

Momentum Space

Contents

The potentials that will be used in this thesis are interactions born in the space called momentum space.
Similar to the more commonly known and used coordinate space, momentum space has its own peculiarities that will set us up in the right path for the creation of our system of coordinates.
In this chapter I will explore the momentum space and how one can build a system of hyperspherical coordinates in this case.
HH calculations have been already carried out in momentum space [25]. In that work the momentum space HH basis was obtained from a Fourier transform of the coordinate space HH basis. For the hyperspherical part one finds that $\mathcal{Y}_{[K_N]}(\Omega_r) \xrightarrow{\text{FT}} \mathcal{Y}_{[K_N]}(\Omega_p)$, whereas the hyperradial basis does not simply lead to Laguerre polynomials in momentum space. This allowed the possibility to calculate at the same time matrix elements of momentum space potentials and coordinate space potentials (e.g. the Coulomb interaction)and simply sum them. However, following such an approach there is an increase in complexity for the momentum space hyperradial part, since the Fourier transform of the Laguerre polynomial is a more complicated hypergeometric function that requires

an enormous amount of precision in the integrations as the required number of polynomials necessary for convergence rises.
The program that I developed in this thesis, instead, uses a system of coordinates that is completely born in momentum space, and it is generated in a similar manner as its coordinate space counterpart. The end result is a program able to use momentum space or real space potentials, and it is able to study systems composed of particles of different masses and/or statistics.
After the proper definition of momentum space basis I will then show results of the benchmark calculations comparing coordinate and momentum space computations for various potential models (Minnesota, Malfliet-Tjon and Ali-Bodmer) and systems (^{3}H,^{3}He and ^{12}C and ^{9}Be in cluster configurations).

3.1 The properties and characteristics of momentum space

Momentum space is defined as the set of all the momentum vectors $\boldsymbol{p}$ a physical system can have.
Is it a space very closely related to the coordinate space, the set of all space position vectors $\boldsymbol{r}$ a system can have. Indeed, the two spaces are connected by what is a called a Pontryagin duality: one can "move" from one space to the other through the use of the operation called Fourier transform, and the three-dimensional vectors $\boldsymbol{p}$ and $\boldsymbol{r}$ are conjugate variables:

$$[r_i^\alpha, p_j^\beta] = i\hbar\delta_{\alpha\beta}\delta_{ij}, \tag{3.1}$$

where $i, j = 1, ..., A$ and $\alpha, \beta = x, y, z$.
Given a distribution $f(\boldsymbol{r})$ in coordinate space, then one can find the equivalent distribution in momentum space, $\psi(\boldsymbol{p})$, through the use of a Fourier transform:

$$\psi(\boldsymbol{p}) = \mathcal{F}(f(\boldsymbol{r})) = \frac{1}{(2\pi)^{\frac{3}{2}}} \int e^{i\boldsymbol{p}\cdot\boldsymbol{r}} f(\boldsymbol{r}) d\boldsymbol{r}. \tag{3.2}$$

We can also calculate the inverse operation, finding $f(\boldsymbol{r})$ from $\psi(\boldsymbol{p})$, through the use of the inverse Fourier transform:

$$f(\boldsymbol{r}) = \mathcal{F}^{-1}(\psi(\boldsymbol{p})) = \frac{1}{(2\pi)^{\frac{3}{2}}} \int e^{-i\boldsymbol{p}\cdot\boldsymbol{r}} \psi(\boldsymbol{p}) d\boldsymbol{p}. \tag{3.3}$$

The Fourier transform is an operation that has been studied for almost two centuries, with many useful properties. However, their explanation is outside the scope of this thesis, so, for the time being, we will consider only a couple of them, the most used and useful ones for this study:

$\mathrm{V}(\boldsymbol{r})$	$\mathrm{V}(\boldsymbol{q})$
$\delta(\boldsymbol{r})$	$\frac{1}{(2\pi)^{\frac{3}{2}}}$
$\nabla^2\delta(\boldsymbol{r})$	$\frac{\boldsymbol{q}^2}{(2\pi)^{\frac{3}{2}}}$
$e^{-\alpha\boldsymbol{r}^2}$	$\left(\sqrt{\frac{\pi}{\alpha}}\right)^3 e^{-\frac{\boldsymbol{q}^2}{4\alpha}}$
$\frac{e^{-\mu\boldsymbol{r}}}{\boldsymbol{r}}$	$\frac{1}{(2\pi)^{\frac{3}{2}}}\frac{4\pi}{\mu^2+\boldsymbol{q}^2}$
$\frac{1}{\boldsymbol{r}}$	$\frac{1}{(2\pi)^{\frac{3}{2}}}\frac{4\pi}{\boldsymbol{q}^2}$

Table 3.1: The most common potentials and relative Fourier transformed form.

- Linearity:

$$\mathcal{F}(af(\boldsymbol{r}) + bg(\boldsymbol{r})) = a\mathcal{F}(f(\boldsymbol{r})) + b\mathcal{F}(g(\boldsymbol{r})). \tag{3.4}$$

- Time scaling:

$$\mathcal{F}(f(\boldsymbol{r})) = \psi(\boldsymbol{p}) \Rightarrow \mathcal{F}(f(a\boldsymbol{r})) = \frac{1}{a^3}\psi\left(\frac{\boldsymbol{p}}{a}\right). \tag{3.5}$$

Then one can see, from the these formulae and properties, that it is possible to transform quite easily the scalar part of a potential $V(\boldsymbol{r})$ in coordinate space in its counterpart in momentum space, $V(\boldsymbol{p})$.

However, the transformed potential is not dependent only on $\boldsymbol{p}$, but it is $V(\boldsymbol{q})$, where $\boldsymbol{q}$ is the transferred momentum $\boldsymbol{q} = \boldsymbol{p} - \boldsymbol{p}'$. Then the hidden difficulty of momentum space potentials is then revealed: the overwhelming majority of them is in a nonlocal form.

In table 3.1 are reported the most common forms of the coordinate space potential $V(\boldsymbol{r})$ and the relative momentum space, Fourier transformed potential $V(\boldsymbol{q})$. As one can see, moving in the momentum space doesn't complicate the 'form' of the potential; indeed one can see in some cases, as the contact interaction, it becomes even simpler, moving from a collection of Dirac deltas to a much more manageable form. However, the aforementioned nonlocality is shown to be present everywhere except the simplest case of a contact potential; it becomes essential then the study of how one can treat such a troublesome form in the Hyperspherical Harmonics formalism.

3.2 The right set of coordinates

As it was introduced in the first section of this chapter, one can easily transform a coordinate space potential in its momentum space equivalent. The transformation will most likely put the aforementioned potential in a nonlocal form, that can still be treated in the HH formalism. The only missing piece now is the choice of the Jacobian coordinates, the link between these two.
As seen before, there is quite a large choice in how $\boldsymbol{r}_1, \boldsymbol{r}_2$, etc., the real space coordinates, can be mixed in order to create a full set of Jacobian coordinates. The same freedom is present also in the case of the momentum space coordinates $\boldsymbol{p}_1, \boldsymbol{p}_2$, etc. However, like in the previous case the right choice in the ordering of the coordinates simplified enormously the calculation by tying only coordinates present in the potentials to $\boldsymbol{\eta}_N$, even in this case there are some peculiar mixing choices that can help in the simplifications of the calculations, and, doing so, in a lighter workload for the calculator.
In the first section it was mentioned how the transformed potential and the EFT potential that will be used are dependent on both $\boldsymbol{p}_{12}$ and its primed counterpart. However $\boldsymbol{p}_{12}$ has a different definition than $\boldsymbol{r}_{12}$; while the latter is defined as simply $\boldsymbol{r}_2 - \boldsymbol{r}_1$, the former, following the definition of conjugate variable, is instead

$$\boldsymbol{p}_{12} = \frac{m_1\boldsymbol{p}_2 - m_2\boldsymbol{p}_1}{M_2} = \frac{m_1\boldsymbol{p}_2 - m_2\boldsymbol{p}_1}{m_1 + m_2}. \tag{3.6}$$

This makes the previous choice of Jacobian coordinates not quite ideal in this case, since we will lack a direct proportionality between a momentum space equivalent of $\boldsymbol{\eta}_N$ (that we will call $\boldsymbol{\pi}_N$) and $\boldsymbol{p}_{12}$ if $m_1 \neq m_2$, the case analyzed in this thesis. This will make a potential V=V($\boldsymbol{p}_{12}$) dependent on more than one Jacobian coordinate after the transformation, increasing by several times the number of integrations necessary for the calculations of matrix elements of the potential, an extremely heavy amount for the calculator.
Another possibility is to start from the definition of momentum. As

$$\boldsymbol{p} = -i\hbar\frac{\partial}{\partial \boldsymbol{r}} \tag{3.7}$$

the momentum space Jacobian coordinates (defined henceforth as $\boldsymbol{\pi}_i$) will be defined as

$$\boldsymbol{\pi}_i = -i\hbar\frac{\partial}{\partial \boldsymbol{\eta}_i} = \sum_{j=1}^{N} -i\hbar\frac{\partial}{\partial \boldsymbol{r}_j}\frac{d\boldsymbol{r}_j}{d\boldsymbol{\eta}_i} = \sum_{j=1}^{N} \boldsymbol{p}_j\frac{d\boldsymbol{r}_j}{d\boldsymbol{\eta}_i}. \tag{3.8}$$

Indeed, the procedure here described is just the generation of the conjugate variables of $\boldsymbol{\eta}_i$:

$$[\eta_i^\alpha, \pi_j^\beta] = i\hbar\delta_{\alpha\beta}\delta_{ij}, \tag{3.9}$$

where $i, j = 1, ..., N$ and $\alpha, \beta = x, y, z$.
In the case analyzed in this thesis, the three body system of particles, this leads to the following result:

$$\begin{aligned}
\boldsymbol{\pi}_2 &= \sqrt{\frac{mM_2}{m_1m_2}}\left(\frac{m_1\boldsymbol{p}_2 - m_2\boldsymbol{p}_1}{M_2}\right) \\
\boldsymbol{\pi}_1 &= \sqrt{\frac{mM_2}{m_3M_3}}\left(\boldsymbol{p}_3 - \frac{m_3}{M_2}(\boldsymbol{p}_1 + \boldsymbol{p}_2)\right) \\
\boldsymbol{\pi}_0 &= \sqrt{\frac{m}{M_3}}(\boldsymbol{p}_1 + \boldsymbol{p}_2 + \boldsymbol{p}_3)
\end{aligned} \tag{3.10}$$

where the direct proportionality between the last Jacobian coordinate ($\boldsymbol{\pi}_2$ in this case) and $\boldsymbol{p}_{12}$ has been restored:

$$\boldsymbol{\pi}_2 = \sqrt{\frac{mM_2}{m_1m_2}}\boldsymbol{p}_{12}. \tag{3.11}$$

The Jacobian determinant for the transformation $(\boldsymbol{p}_1, \boldsymbol{p}_2, \boldsymbol{p}_3) \rightarrow (\boldsymbol{\pi}_0, \boldsymbol{\pi}_1, \boldsymbol{\pi}_2)$ is the opposite as the coordinate space one

$$\mathcal{J} = \prod_{i=1}^{3}\sqrt{\frac{m}{m_i}}. \tag{3.12}$$

After the determination of the Jacobian coordinates, the move to hyperspherical coordinates and the construction of the HH functions is the same as described in the second chapter, so, to distinguish between the two spaces from here on I will use Q to specifically describe the momentum space hyperradius. The only notable difference is present in the construction of the kinetic energy operator. While in the previous case in real space the internal kinetic energy of the system would be calculated from a quite complicated hyperlaplacian, in momentum space the calculation of the internal kinetic energy is a much simpler matter.
In the three body case the total kinetic energy is

$$T_{total} = \sum_{i=1}^{3}\frac{p_i^2}{2m_i}, \tag{3.13}$$

that can be written in Jacobian coordinates, by using the inverse transformation of Eq. (3.11):

$$\begin{aligned}
\boldsymbol{p}_1 &= \sqrt{\frac{m_1}{m}}\left(\sqrt{\frac{m_1}{M_3}}\boldsymbol{\pi}_0 - \sqrt{\frac{m_1 m_3}{M_3 M_2}}\boldsymbol{\pi}_1 - \sqrt{\frac{m_1}{M_2}}\boldsymbol{\pi}_2\right) \\
\boldsymbol{p}_2 &= \sqrt{\frac{m_2}{m}}\left(\sqrt{\frac{m_2}{M_3}}\boldsymbol{\pi}_0 - \sqrt{\frac{m_2 m_3}{M_3 M_2}}\boldsymbol{\pi}_1 + \sqrt{\frac{m_1}{M_2}}\boldsymbol{\pi}_2\right) \\
\boldsymbol{p}_3 &= \sqrt{\frac{m_3}{m}}\left(\sqrt{\frac{m_3}{M_3}}\boldsymbol{\pi}_0 + \sqrt{\frac{M_2}{M_3}}\boldsymbol{\pi}_1\right)
\end{aligned} \tag{3.14}$$

obtaining the following nice, compact result:

$$T_{total} = \frac{\pi_0^2 + \pi_1^2 + \pi_2^2}{2m} \tag{3.15}$$

The internal kinetic energy is defined as

$$T_{int} = T_{total} - T_{CM} = T_{total} - \frac{P_{CM}^2}{2M_3} = T_{total} - \frac{(p_1 + p_2 + p_3)^2}{2M_3}, \tag{3.16}$$

inserting Eq. (3.11) and (3.15) in this definition, one gets the following result

$$T_{int} = \frac{\pi_1^2 + \pi_2^2}{2m} \tag{3.17}$$

Finally, remembering that, in momentum space in a three body system, the hyperradius Q is defined in a similar manner as its real space counterpart ρ, as

$$Q = \sqrt{\boldsymbol{\pi}_1^2 + \boldsymbol{\pi}_2^2} \tag{3.18}$$

one obtains the following, extremely simple, formula to calculate the internal kinetic energy:

$$T_{int} = \frac{Q^2}{2m}. \tag{3.19}$$

3.3 Nonlocal potential in the HH formalism

We want to calculate the following matrix element of a nonlocal potential in a HH basis

$$V_{12,mn} = \langle \Psi_{[m]} | V(p_{12}, p'_{12}) | \Psi_{[n]} \rangle \tag{3.20}$$

where $[m]$ and $[n]$ are sets of quantum numbers. In order to obtain this, we first define our basis wavefunction Ψ as a product of purely hyperradial function and a purely hyperangular one:

$$\Psi_{[n]}(\boldsymbol{\pi}_1, ..., \boldsymbol{\pi}_N) = \Psi_{[n]}(Q, \Omega_{(N)}) = g_n(Q)\mathcal{Y}_{[K_n]}(\Omega_{(N)}) \tag{3.21}$$

with $g_n(Q)$ defined as

$$g_n(Q) = \sqrt{\frac{n!}{(n+\nu)!}} Q^{\frac{\nu}{2} - \frac{3n-1}{2}} e^{-\frac{Q}{2}} L_n^\nu(Q) \tag{3.22}$$

and $\mathcal{Y}_{[K_n]}(\Omega_{(N)})$ the hyperspherical harmonic of the full system, with set of hyperangular quantum numbers $[K_N]$. Such a function can be decomposed, as seen in the second chapter, in the following way:

$$\begin{aligned} \mathcal{Y}_{[K_N]}(\Omega_{(N)}) =& \mathcal{N}(K_N; l_N K_{N-1})(\sin\Phi_N)^{l_n}(\cos\Phi_N)^{K_N} \times \\ & \times P_{n_N}^{(l_N+\frac{1}{2}, K_{N-1}+\frac{3N-5}{2})}(\cos(2\Phi_N)) \times \\ & \times \sum_{M_N, m_N} (\langle L_{N-1} M_{N-1} l_N m_N | L_N M_N \rangle \times \\ & \times \mathcal{Y}_{[K_{N-1}]}(\Omega_{(N-1)}) Y_{l_N}^{m_N}(\Omega_N)). \end{aligned} \tag{3.23}$$

Before calculating the value of this integral I need to take another little step, though.
As described in the previous sections of this chapter, when moving from a set of Cartesian coordinates to a set of Jacobian ones to a set of hyperspherical ones we make the following transformations:

$$(\boldsymbol{p}_1, ..., \boldsymbol{p}_A) \to (\boldsymbol{\pi}_1, ..., \boldsymbol{\pi}_N) \to (Q, \Phi_2, ..., \Phi_N, \varphi_1, ..., \varphi_N, \theta_1, ..., \theta_N) \to (Q, \Omega_{(N)}) \tag{3.24}$$

However in this case the potential is nonlocal, meaning that it is dependent not only on the distance p_{12} but also on p'_{12}. Then we need to define a new set of Jacobian coordinates $(\boldsymbol{\pi}_1, ..., \boldsymbol{\pi}_N, \boldsymbol{\pi}'_N)$ to reflect the added variable. Then our nonlocal potential becomes $V = V(\boldsymbol{\pi}_N, \boldsymbol{\pi}'_N)$. However we need to reflect this change also in the hyperspherical basis; by definition we have

$$\begin{cases} \pi_N = Q \sin(\Phi_N) \\ \Omega_N = (\varphi_N, \theta_N) \end{cases} \tag{3.25}$$

with

$$Q = \sum_{i=1}^{N} \pi_i^2 \tag{3.26}$$

Then we can, in the same fashion, define four other variables:

$$\begin{cases} \pi'_N = Q' \sin(\Phi'_N) \\ \Omega'_N = (\varphi'_N, \theta'_N) \end{cases} \tag{3.27}$$

with

$$Q' = \sum_{i=1}^{N-1} \pi_i^2 + \pi_N'^2 \tag{3.28}$$

However this gives rise to a little problem. The addition of $\boldsymbol{\pi}'_N$ gave us three more variables, while we have just defined four. Luckily this discrepancy can be easily solved by noting that there is a relation present between two of the four variables. Using Eq. (3.27) together with Eq. (3.28) one obtains the following:

$$Q'^2 = \sum_{i=1}^{N-1} \pi_i^2 + \pi_N'^2 = \sum_{i=1}^{N-1} \pi_i^2 + Q'^2 \sin^2(\Phi'_N) \Rightarrow \sum_{i=1}^{N-1} \pi_i^2 = Q'^2(1 - \sin^2(\Phi'_N)) \tag{3.29}$$

Then one can make the same reasoning with Eq. (3.25) and Eq. (3.26), obtaining

$$\sum_{i=1}^{N-1} \pi_i^2 = Q^2(1 - \sin^2(\Phi_N)) = Q^2 \cos^2(\Phi_N) \tag{3.30}$$

Putting the two results together

$$Q^2 \cos^2(\Phi_N) = Q'^2 \cos^2(\Phi'_N) \Rightarrow \cos^2(\Phi'_N) = \cos^2(\Phi_N) \frac{Q^2}{Q'^2} \tag{3.31}$$

we obtain a relation with which we can remove Φ'_N as a free variable in the integration. However one needs to pay attention for the consequences that this act involves: when one moves from the Jacobian set of coordinates to the hyperspherical one there is a new element of volume to add that cannot be simply obtained by mirroring the relation used for Q and Φ_N. Indeed, we have to make the following transformations:

$$\boldsymbol{\pi}'_N = (\pi'_{N_x}, \pi'_{N_y}, \pi'_{N_z}) \rightarrow (\pi'_N, \varphi'_N, \theta'_N) \rightarrow (Q', \varphi'_N, \theta'_N). \tag{3.32}$$

While the first one is a simple movement from the Cartesian coordinates to the spherical ones, the second one is a little more tricky. In the second set the volume element is

$$dV = \pi'_N d\pi'_N d\Omega'_N \tag{3.33}$$

so we need to transform it using Eq. (3.27) but keeping in mind the relation (3.31). Doing so will result in the following:

$$\begin{aligned} d\pi'_N &= d(Q' \sin(\Phi'_N) = d(Q' \sqrt{1 - \cos^2(\Phi'_N)}) = \\ &= d\left(Q' \sqrt{1 - \cos^2(\Phi_N) \frac{Q^2}{Q'^2}} \right) = d(\sqrt{Q'^2 - Q^2 \cos^2(\Phi_N)}) = \\ &= \frac{2Q'}{2\sqrt{Q'^2 - Q^2 \cos^2(\Phi_N)}} dQ' = \frac{dQ'}{\sqrt{1 - \frac{Q^2}{Q'^2} \cos^2(\Phi_N)}} = \frac{dQ'}{\sin(\Phi'_N)} \end{aligned} \tag{3.34}$$

meaning that the final element of volume will be

$$dV = \pi_N'^2 d\pi_N' = Q'^2 \sin^2(\Phi_N') \frac{dQ'}{\sin(\Phi_N')} = Q'^2 \sin(\Phi_N') dQ' \tag{3.35}$$

From here one can rewrite integral (3.20) in HH coordinates as

$$\begin{aligned} V_{mn} = \mathcal{N} \int & dQ dQ' d\Phi_N d\Omega_{(N-1)} d\Omega_N d\Omega_N' Q^{3N-1} Q'^2 g_m(Q) g_n(Q') \times \\ & \times (\sin(\Phi_N))^{l_N+2} (\cos(\Phi_N))^{K_{N-1}+3N-4} P_{n_N}^{(l_n+\frac{1}{2}, K_{N-1}+\frac{3N-5}{2})} (\cos(2\Phi_N)) \times \\ & \times \sum_{M_{N-1}, m_N} (\langle L_{N-1} M_{N-1} l_N m_N | L_N M_N \rangle \mathcal{Y}_{[K_{N-1}]}(\Omega_{(N-1)}) Y_{l_N}^{m_N}(\Omega_N)) \times \\ & \times V(\boldsymbol{\pi}_N, \boldsymbol{\pi}_N') (\sin(\Phi_N'))^{l_N'+1} (\cos(\Phi_N'))^{K_{N-1}'} P_{n_N'}^{(l_n'+\frac{1}{2}, K_{N-1}'+\frac{3N-5}{2})} (\cos(2\Phi_N')) \times \\ & \times \sum_{M_{N-1}', m_N'} (\langle L_{N-1}' M_{N-1}' l_N' m_N' | L_N' M_N' \rangle \mathcal{Y}_{[K_{N-1}']}(\Omega_{(N-1)}) Y_{l_N'}^{m_N'*}(\Omega_N')) \end{aligned} \tag{3.36}$$

with $\mathcal{N} = \mathcal{N}(K_N, l_N, K_{N-1}) \mathcal{N}(K_N', l_N', K_{N-1}')$ the product of all normalization factors of the various functions in the integrand.
The best way to calculate this integral is in steps:

1. Calculate the integral in $\Omega_{(N-1)}$
2. Calculate the integral in the remaining angles except Φ_N (Ω_N and Ω_N')
3. Finish the calculation in Φ_N, Q and Q'

The first one is the easiest to complete, since the only functions dependent on $\Omega_{(N-1)}$ are the hyperspherical harmonics $\mathcal{Y}_{[K_{N-1}]}$ and $\mathcal{Y}_{[K_{N-1}']}$. As seen before the integral will give a very simple result:

$$\int d\Omega_{(N-1)} \mathcal{Y}_{[K_{N-1}]}(\Omega_{(N-1)}) \mathcal{Y}_{[K_{N-1}']}(\Omega_{(N-1)}) = \delta_{[K_{N-1}][K_{N-1}']} \tag{3.37}$$

This means that the integral in Eq. (3.36) can be reduced to

$$\begin{aligned} V_{mn} = \mathcal{N} \int & dQ dQ' d\Phi_N d\Omega_N d\Omega_N' Q^{3N-1} Q'^2 g_m(Q) g_n(Q') \times \\ & \times (\sin(\Phi_N))^{l_N+2} (\cos(\Phi_N))^{K_{N-1}+3N-4} P_{n_N}^{(l_n+\frac{1}{2}, K_{N-1}+\frac{3N-5}{2})} (\cos(2\Phi_N)) \times \\ & \times \sum_{M_{N-1}, m_N} (\langle L_{N-1} M_{N-1} l_N m_N | L_N M_N \rangle Y_{l_N}^{m_N}(\Omega_N)) \times \\ & \times V(\boldsymbol{\pi}_N, \boldsymbol{\pi}_N') (\sin(\Phi_N'))^{l_N'+1} (\cos(\Phi_N'))^{K_{N-1}'} P_{n_N'}^{(l_n'+\frac{1}{2}, K_{N-1}'+\frac{3N-5}{2})} (\cos(2\Phi_N')) \times \\ & \times \sum_{M_{N-1}', m_N'} (\langle L_{N-1} M_{N-1} l_N' m_N' | L_N' M_N' \rangle Y_{l_N'}^{m_N'*}(\Omega_N')) \delta_{[K_{N-1}][K_{N-1}']}. \end{aligned} \tag{3.38}$$

Now we need to tackle the second point in the list, the integration in the angles Ω_N and Ω'_N. This is a set of four angles, result of moving the Jacobian coordinates from a set of Cartesian-like coordinates to a spherical one.
Usually the integration in these angles will simply give a delta in the last set of angular quantum numbers (L_N and M_N), however in this case we have also the potential in the integrand. This increase the total number of integrations required by four, making the calculations of the matrix elements much longer and problematic.
However there is a technique we can use to reduce this problematic calculation to a more manageable size.

3.3.1 The Euler angles

The non-locality of the potential raises the number of dimensions of the final integral, adding to Φ_N and (Q, Ω_N) the three dimensional (Q', Ω'_N), increasing greatly the computational load on the calculation. A solution is to choose Euler angles, representing rotations of the system as a whole, as three of the seven degrees of freedom and carry out the integration as a whole. The following procedure was introduced by V.D. Efros as a method for the elimination of rotational degrees of freedom in the expansion method for three nucleons in [26].
We first consider two three dimensional vectors, they could be $\boldsymbol{\pi_N}$ and $\boldsymbol{\pi'_N}$ or (Q, Ω_N) and (Q', Ω'_N). For simplicity we will call them $\boldsymbol{u} = (u_x, u_y, u_z)$ and $\boldsymbol{v} = (v_x, v_y, v_z)$.
We consider three-dimensional rotations over the three Euler angles (from now on collectively denoted by ω) as rotations of the whole system of coordinates, moving the vectors $\boldsymbol{u}$, $\boldsymbol{v}$ to the new vectors $\boldsymbol{u'}$, $\boldsymbol{v'}$ in the new system. Then, given some spatial components $F_{LM}(\boldsymbol{u}, \boldsymbol{v})$ of some basis functions for our system (where L and M are respectively the orbital momentum and its projection quantum numbers), its transformation under rotation is the following

$$F_{LM'}(\boldsymbol{u'}, \boldsymbol{v'}) = \sum_{M=-L}^{L} D^L_{MM'}(\omega) F_{LM}(\boldsymbol{u}, \boldsymbol{v}) \tag{3.39}$$

where $D^L_{MM'}$ are the Wigner D-functions.
One can also use the inverse relation

$$F_{LM}(\boldsymbol{u}, \boldsymbol{v}) = \sum_{M'=-L}^{L} D^{L*}_{MM'}(\omega) F_{LM'}(\boldsymbol{u'}, \boldsymbol{v'}) \tag{3.40}$$

to choose a new coordinate system in a way that it corresponds to a body reference frame associated with the plane generated by the vectors $\boldsymbol{u}$ and $\boldsymbol{v}$.

In this way one can express the various coordinates $\boldsymbol{u}'_i$ and $\boldsymbol{v}'_i$ in terms of the scalar quantities u, v, and $\boldsymbol{u} \cdot \boldsymbol{v}$. In this way the previous expression becomes an expansion of F_{LM} over D-functions with coefficients depending on scalar coordinates.
Since we're free to choose the orientation of the body reference frame with respect to the laboratory reference frame, we can use the convenient choice of directing the z axis of the body reference frame along the vector $\boldsymbol{u}$, and to place the x axis on the $\boldsymbol{u} - \boldsymbol{v}$ plane in a way that gives us a positive projection of $\boldsymbol{v}$ along this axis. With this we obtain the following simplifications:

$$u'_x = 0 \quad u'_y = 0 \quad u'_z = u \quad v'_x = v\sqrt{1-t^2} \quad v'_y = 0 \quad v'_z = vt \tag{3.41}$$

where $t = \hat{u} \cdot \hat{v}$. Then equation (3.40) becomes

$$F_{LM}(\boldsymbol{u}, \boldsymbol{v}) = \sum_{M'=-L}^{L} D^{L*}_{MM'}(\omega) F_{LM'}(u, v, t) \tag{3.42}$$

with

$$F_{LM'}(u, v, t) = F_{LM'}(u'_z = 0, u'_y = 0, u'_z = u, v'_z = v\sqrt{1-t^2}, v'_y = 0, v'_z = vt). \tag{3.43}$$

Suppose now that we want to calculate the following integral

$$\int d\boldsymbol{u} d\boldsymbol{v} G_{LM}(\boldsymbol{u}, \boldsymbol{v}) \hat{O}_{u,v,t} F_{LM}(\boldsymbol{u}, \boldsymbol{v}) \tag{3.44}$$

where F and G are functions and $\hat{O}$ an operator.
Then one can introduce the previous relations together with a change of variables (from $(\boldsymbol{u}, \boldsymbol{v})$ to $(\omega = \{\alpha, \beta, \gamma\}, u, v, t)$). The previous integral in Eq. (3.44) over the Euler angles can then be calculated analytically (see [26]), leading to the following expression:

$$\delta_{MM'} \delta_{LL'} \frac{8\pi}{2L+1} \int du\, dv\, dt\, u^2 v^2 \sum_{M''=-L}^{L} G_{LM''}(u, v, t) \hat{O}_{u,v,t} F_{LM''}(u, v, t). \tag{3.45}$$

We can then get back to the Eq. (3.38). Using, instead of $\boldsymbol{u}$ and $\boldsymbol{v}$, the coordinates $\boldsymbol{\pi_N}$ and $\boldsymbol{\pi'_N}$ and as the F and G the remaining functions of equation (3.38), with the potential as the operator. Remembering that, after the rotation, the angles $(\Omega_N, \Omega'_N) = (\theta_N, \varphi_N, \theta'_N, \varphi'_N)$ become $(0, 0, \arccos(\hat{u} \cdot \hat{v}) = \arccos(t), 0)$ we have

that Eq.(3.38) becomes:

$$
\begin{aligned}
V_{mn} = \frac{8\pi^2}{2l_n+1}\mathcal{N}\int dQdQ'Q^{3N-1}Q'^2 g_m(Q)g_n(Q')\times \\
\times \int d\Phi_N(\sin\Phi_N)^{l_N+2}(\cos\Phi_N)^{K_{N-1}+3N-4}P_{n_N}^{(l_N+\frac{1}{2},K_{N-1}+\frac{3N-5}{2})}(\cos(2\Phi_N))\times \\
\times (\sin\Phi'_N)^{l_N+1}(\cos\Phi'_N)^{K'_{N-1}}P_{n_N}^{(l_N+\frac{1}{2},K_{N-1}+\frac{3N-5}{2})}(\cos(2\Phi'_N))\times \\
\times \int dt \sum_{M_{N-1},m_N}\sum_{M'_{N-1},m'_N}\langle L_{N-1}M_{N-1}l'_Nm'_N|L'_NM'_N\rangle\langle L_{N-1}M_{N-1}l_Nm_N|L_NM_N\rangle\times \\
\times \sum_{m''_N=-l_N}^{l_N} Y_{l_N}^{m''_N}(0,0)V(\pi_N,\pi'_N,t)Y_{l_N}^{m''_N}(\arccos(t),0)\delta_{[K_{N-1}][K'_{N-1}]}\delta_{l_Nl'_N}\delta_{m_Nm'_N} = \qquad (3.46)\\
= \delta_{[K_{N-1}][K'_{N-1}]}\delta_{l_Nl'_N}\delta_{m_Nm'_N}\mathcal{N}\int dQdQ'Q^{3N-1}Q'^2 g_m(Q)g_n(Q')\times \\
\times \int d\Phi_N(\sin\Phi_N)^{l_N+2}(\cos\Phi_N)^{K_{N-1}+3N-4}P_{n_N}^{(l_N+\frac{1}{2},K_{N-1}+\frac{3N-5}{2})}(\cos(2\Phi_N))\times \\
\times (\sin\Phi'_N)^{l_N+1}(\cos\Phi'_N)^{K'_{N-1}}P_{n_N}^{(l_N+\frac{1}{2},K_{N-1}+\frac{3N-5}{2})}(\cos(2\Phi'_N))\times \\
\times \sum_{M_{N-1},m_N}\langle L_{N-1}M_{N-1}l_Nm_N|L_NM_N\rangle\langle L_{N-1}M_{N-1}l_Nm_N|L'_NM'_N\rangle\times \\
\times \frac{8\pi}{2l_N+1}\sum_{m''_N=-l_N}^{l_N}\int dtY_{l_N}^{m''_N}(0,0)V(\pi_N,\pi'_N,t)Y_{l_N}^{m''_N}(\arccos(t),0). \qquad (3.47)
\end{aligned}
$$

We obtained a non-negligible simplification of the previous integral, but, with some additional observations, we can do better.
Let's look at the first integral that we need to make

$$\int dtY_{l_N}^{m''_N}(0,0)V(\pi_N,\pi'_N,t)Y_{l_N}^{m''_N}(\arccos(t),0) \qquad (3.48)$$

The spherical harmonic function $Y_l^m(\theta,\phi)$ can be written in the following way:

$$Y_l^m(\theta,\phi) = (-1)^m\sqrt{\frac{2l+1}{4\pi}\frac{(l-m)!}{(l+m)!}}P_l^m(\cos(\theta))e^{im\phi}, \qquad (3.49)$$

where P_l^m is the associated Legendre polynomial. Inserting this definition in the matrix element integral we obtain

$$\frac{2l_N+1}{4\pi}\frac{(l-m''_N)!}{(l+m''_N)!}\int_0^1 dtP_{l_N}^{m''_N}(1)V(\pi_N,\pi'_N,t)P_{l_N}^{m''_N}(t). \qquad (3.50)$$

Remembering that the associated Legendre polynomial is defined as

$$P_l^m(x) = (-1)^m(1-x^2)^{\frac{m}{2}}\frac{d^m}{dx^m}(P_l(x)) \qquad (3.51)$$

where $P_l(x)$ is the ordinary Legendre polynomial, we can see that

$$P_l^m(1) = (-1)^m(1-1)^{\frac{m}{2}}\frac{d^m}{dx^m}(P_l(1)) = \delta_{m0} \tag{3.52}$$

and, using it in the previous equation,

$$\int dt Y_{l_N}^{m''_n}(0,0)V(\pi_N,\pi'_N,t)Y_{l_N}^{m''_N}(\arccos t,0) = \delta_{mn}\frac{2l_N+1}{4\pi}\int_{-1}^{1} dt V(Q,\rho',t)P_{l_N}^0(t). \tag{3.53}$$

Defining a new, angular momentum dependent, potential

$$V_{l_N}(\pi_N,\pi'_N) = \int_{-1}^{1} dt V(\pi_N,\pi'_N,t)P_{l_N}^0(t) \tag{3.54}$$

we can write the new form of our matrix element

$$\begin{aligned}
V_{mn} &= \delta_{[K_{N-1}][K'_{N-1}]}\delta_{l_N l'_N}\delta_{m_N m'_N}\mathcal{N}\int dQdQ'Q^{3N-1}Q'^2 g_m(Q)g_n(Q')\times \\
&\times \int d\Phi_N(\sin\Phi_N)^{l_N+3N-4}(\cos\Phi_N)^{K_{N-1}+2}P_{n_N}^{(l_N+\frac{1}{2},K_{N-1}+\frac{3N-5}{2})}(\cos(2\Phi_N))\times \\
&\times (\sin\Phi'_N)^{l_N+1}(\cos\Phi'_N)^{K'_{N-1}}P_{n_N}^{(l_N+\frac{1}{2},K_{N-1}+\frac{3N-5}{2})}(\cos(2\Phi'_N))\times \\
&\times \sum_{M_{N-1},m_N}\langle L_{N-1}M_{N-1}l_N m_N|L_N M_N\rangle\langle L_{N-1}M_{N-1}l_N m_N|L'_N M'_N\rangle\times \\
&\times \frac{8\pi}{2L+1}\delta_{m''0}\frac{2l_N+1}{4\pi}V_{l_N}(\pi_N,\pi'_N) = \\
&= \delta_{[K_{N-1}][K'_{N-1}]}\delta_{l_N l'_N}\delta_{m_N m'_N}\delta_{m''0}2\pi\mathcal{N}\int dQdQ'Q^{3N-1}Q'^2 g_m(Q)g_n(Q')\times \\
&\times \int d\Phi_N(\sin\Phi_N)^{l_N+2}(\cos\Phi_N)^{K_{N-1}+3N-4}P_{n_N}^{(l_N+\frac{1}{2},K_{N-1}+\frac{3N-5}{2})}(\cos(2\Phi_N))\times \\
&\times (\sin\Phi'_N)^{l_N+1}(\cos\Phi'_N)^{K'_{N-1}}P_{n_N}^{(l_N+\frac{1}{2},K_{N-1}+\frac{3N-5}{2})}(\cos(2\Phi'_N))\times \\
&\times \sum_{M_{N-1},m_N}\langle L_{N-1}M_{N-1}l_N m_N|L_N M_N\rangle\langle L_{N-1}M_{N-1}l_N m_N|L'_N M'_N\rangle V_{l_N}(\pi_N,\pi'_N).
\end{aligned} \tag{3.55, 3.56}$$

For the final observation we note the following property of the Clebsch-Gordan coefficients:

$$\sum_{m_1=-j_1}^{j_1}\sum_{m_2=-j_2}^{j_2}\langle j_1 m_1 j_2 m_2|jm\rangle\langle j_1 m_1 j_2 m_2|j'm'\rangle = \delta_{jj'}\delta_{mm'} \tag{3.57}$$

Introducing this equation in our previous one (with $L_{N-1} = j_1, M_{N-1} = m_1, l_N = j_2, m_N = m_2, L_N = j, M_N = m, L'_N = j'$ and $M'_N = m'$) we can

obtain the final form of our non-local matrix element:

$$
\begin{aligned}
V_{mn} = {} & \delta_{[K_{N-1}][K'_{N-1}]}\delta_{l_N l'_N}\delta_{m_N m'_N}\delta_{L_N L'_N}\delta_{M_N M'_N}\delta_{m''0}\times \\
& \times 2\pi\mathcal{N}\int dQdQ'Q^{3N-1}Q'^2 g_m(Q)g_n(Q')\times \\
& \times \int d\Phi_N(\sin\Phi_N)^{l_N+2}(\cos\Phi_N)^{K_{N-1}+3N-4}P_{n_N}^{(l_N+\frac{1}{2},K_{N-1}+\frac{3N-5}{2})}(\cos(2\Phi_N))\times \\
& \times (\sin\Phi'_N)^{l_N+1}(\cos\Phi'_N)^{K'_{N-1}}P_{n_N}^{(l_N+\frac{1}{2},K_{N-1}+\frac{3N-5}{2})}(\cos(2\Phi'_N))V_{l_N}(\pi_N,\pi'_N).
\end{aligned}
\tag{3.58}
$$

3.4 Benchmarks

Using the HH in momentum space frame described as in chapter 3, the code, scope of this thesis, was developed.
Using a Laguerre quadrature for the hyperradial coordinate Q and a Jacobi one for the hyperangular part, this program creates the two-body potential matrix V_{12}. Successively such a matrix is transformed into the other two-body potential matrices (V_{23},V_{13}, etc.) through the use of the permutation matrices defined in Eq.(2.22). The complete potential matrix is then added to the complete internal kinetic matrix T, derived from the simple formula discussed at the end of the second section. The lowest eigenvalues and eigenstates of the matrix are then obtained through the Lanczos procedure of diagonalization.
The number of hyperradial Laguerre functions, after a study of convergence, has been settled at 30 during all the tests. Increasing the number of polynomials is detrimental to both the speed and the precision (with the introduction of higher-frequency functions) of the calculation, with no discernible difference in the final result with thirty polynomials.
The increase in the number of nested integrations, given by the non-locality of the potential, increases the number of necessary grid points in the hyperradial coordinate's integrations in order to reach convergence, up to 250 points in a classical Laguerre quadrature method of integration. The number of points in the grid necessary for the integration of the hyperangular Jacobi polynomials was instead set to 150.
The first benchmark is a comparison, in the tritium system, between a local potential in coordinate space and its counterpart in momentum space. The first interaction that has been used is a Minnesota potential[27]:

$$V_{\text{Minn}} = V_{S=0} + V_{S=1} \tag{3.59}$$

with

$$\begin{cases} V_{S=0}(r) = V_1 e^{-\mu_1 r^2} + V_2 e^{-\mu_2 r^2} \\ V_{S=1}(r) = V_1 e^{-\mu_1 r^2} + V_3 e^{-\mu_3 r^2} \end{cases} \tag{3.60}$$

in coordinate space and

$$\begin{cases} V_{S=0}(p-p') = \frac{V_1}{8(\pi\mu_1)^{\frac{3}{2}}} e^{-\frac{(p-p')^2}{4\mu_1}} + \frac{V_2}{8(\pi\mu_2)^{\frac{3}{2}}} e^{-\frac{(p-p')^2}{4\mu_2}} \\ V_{S=1}(p-p') = \frac{V_1}{8(\pi\mu_1)^{\frac{3}{2}}} e^{-\frac{(p-p')^2}{4\mu_1}} + \frac{V_3}{8(\pi\mu_3)^{\frac{3}{2}}} e^{-\frac{(p-p')^2}{4\mu_3}} \end{cases} \tag{3.61}$$

in momentum space, the constants V_i and μ_i being

$$\begin{cases} V_1 = 200MeV \\ V_2 = -178MeV \\ V_3 = -91.85MeV \end{cases} \tag{3.62}$$

$$\begin{cases} \mu_1 = 1.487fm^{-2} \\ \mu_2 = 0.639fm^{-2} \\ \mu_3 = 0.465fm^{-2} \end{cases}. \tag{3.63}$$

As one can see in figure 3.1 the result of the computation, for every value of the total hypermomentum K is almost identical in both spaces. The difference is so minimal that it is not visible in the graph, since it amounts to less than a keV, less than a part in ten thousand on the final result. This first benchmark shows the symmetry between the two spaces and serves as the first stepping stone in the generation of the final program. The next step occurs in adding to the soft Minnesota potential an harder part composed of Coulomb repulsion, using this new interaction in the study of the ^{3}He ground state.
As shown in the first section of this chapter, the Yukawa type potential

$$V(r) = \frac{e^{-\mu r}}{r} \tag{3.64}$$

transforms in its momentum space counterpart as

$$V(p-p') = \frac{1}{2\pi^2} \frac{1}{\mu^2 + (p-p')^2}. \tag{3.65}$$

This means that, taking $\mu = 0$, one can easily get the momentum counterpart of the Coulomb potential:

$$V(r) = \frac{e^2}{r} \iff V(p-p') = \frac{1}{2\pi^2} \frac{e^2}{(p-p')^2}, \tag{3.66}$$

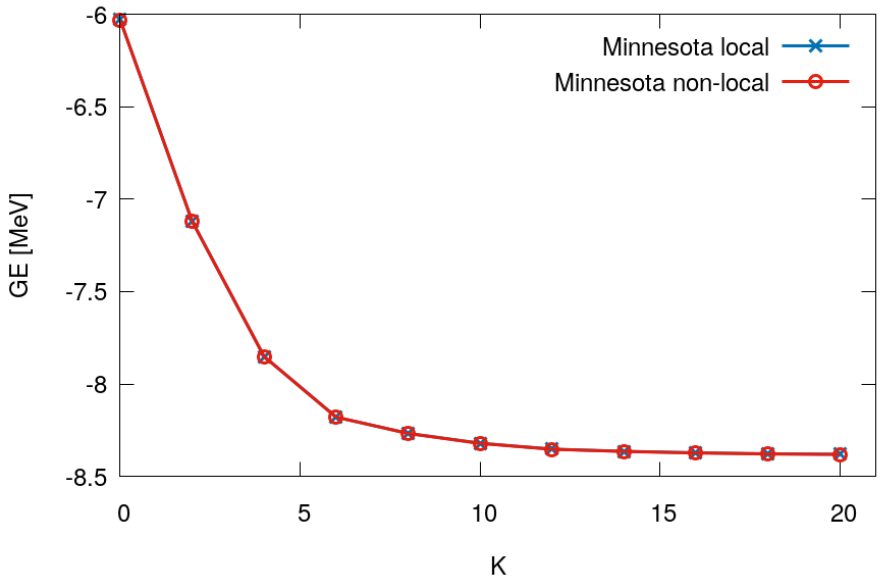

Figure 3.1: Comparison between the calculations of the ground state of tritium with a Minnesota potential and its momentum space counterpart.

with $e^2 \simeq 1.44$ MeV $\cdot$ fm.

The results of the computation are given in figure 3.2, showing once again the symmetry between the two spaces. However, in this case, it was necessary to increase by quite a lot the number of points in the Laguerre grid for the momentum part in order to reach convergence. The hard divergence given by the Coulomb potential required the increase up to 500 points of grid, since with the standard 250 points there was a small but important difference of 0.02 MeV at $K = 20$.

The second potential used for a comparison between spaces of the ground state of tritium is a Malfliet-Tjon potential[28]. Being made of a sum of Yukawa-type potentials, compared to the sum of softer Gaussians that generate the Minnesota potential, this potential should be in principle harder to calculate in momentum space for the program.

The potential presents two components

$$V_{MT13} = V_{S=0} + V_{S=1} \tag{3.67}$$

with

$$\begin{cases} V_{S=0}(r) = V_1 \frac{e^{-\mu_1 r}}{r} - V_2 \frac{e^{-\mu_2 r}}{r} \\ V_{S=1}(r) = V_1 \frac{e^{-\mu_1 r}}{r} - V_3 \frac{e^{-\mu_2 r}}{r} \end{cases} \tag{3.68}$$

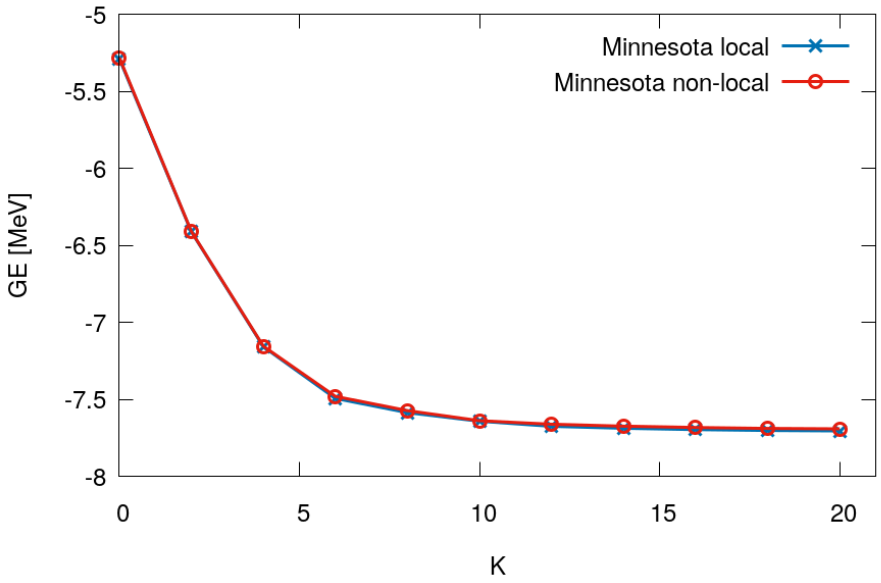

Figure 3.2: Comparison between the calculations of the ground state of ^{3}He with a Minnesota plus a Coulomb interaction and its momentum space counterpart.

in coordinate space and

$$\begin{cases} V_{S=0}(p-p') = \frac{1}{2\pi^2}\left(\frac{V_1}{\mu_1^2+(p-p')^2} - \frac{V_2}{\mu_2^2+(p-p')^2}\right) \\ V_{S=1}(p-p') = \frac{1}{2\pi^2}\left(\frac{V_1}{\mu_1^2+(p-p')^2} - \frac{V_3}{\mu_2^2+(p-p')^2}\right) \end{cases} \tag{3.69}$$

in momentum space, with $V_1 = 1458.047$ MeV, $V_2 = 520.872$ MeV, $V_3 = 635.306$ MeV, $\mu_1 = 3.11$ fm^{-2} and $\mu_2 = 1.555$ fm^{-2}. The results of the computation, up to $K = 20$, are represented in figure 3.3.

The momentum space result, like the previous case of Minnesota plus Coulomb, required an expanded grid up to 500 points, since the 250 points grid result presented more than half a MeV difference from the local result, given by the difficulty of convergence for the numerical integration of the Yukawa potential.

After the checks on the simplest and most commonly used systems for benchmarks, the tritium and ^{3}He nuclei, the next benchmark focuses on the capability of the program to work with different masses M other than the reference mass m. In this case the new system analyzed is the nucleus of Carbon-12, one of the protagonists of this thesis.

Made of six protons and six neutrons, the structure of ^{12}C is that of a cluster nucleus made of three identical substructures, in this case α particles.

As I will explain more at length in the next chapter, using cluster EFT we can represent the three alphas as point-like bosons with mass $M = m_\alpha$. In such

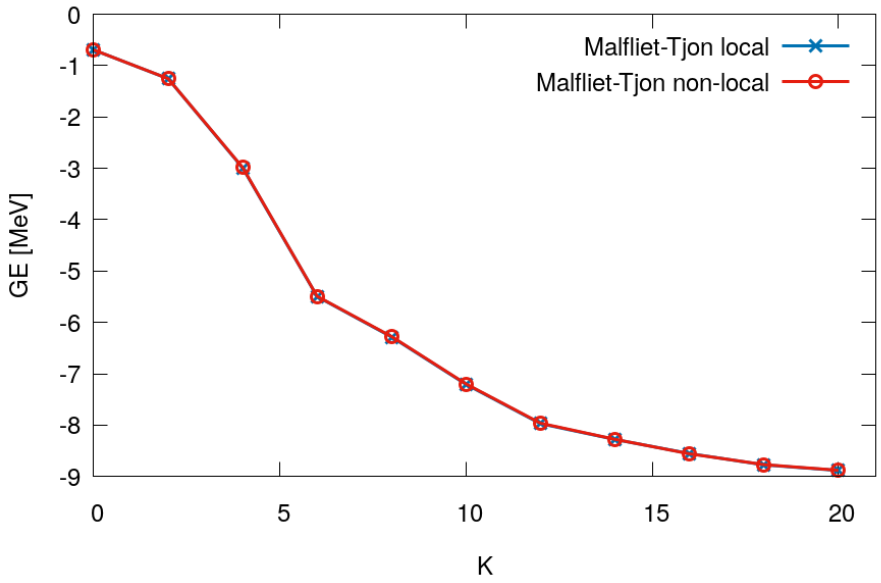

Figure 3.3: Comparison between the calculations of the ground state of tritium with a Malfliet-Tjon interaction and its momentum space counterpart.

a cluster approximation Carbon-12 becomes rather similar to tritium, differing only for particle mass, charge and spin-isospin particle statistics while maintaining the same general structure as a nucleus composed of three indistinguishable particles. Therefore Carbon-12 calculation was rather easy to implement and it could be used as a testing ground both for the cluster EFT potentials and for the nonlocal, momentum space configuration introduced for the first time in the program.

Being the α-particle a spin zero particle, this benchmark will test the capability of the program to handle bosons, that require a different choice in the type and number of states in the basis, being the spin=1 triplet states, usually taken into account (like in the previous cases) not present in this peculiar system.

The interaction used for this benchmark is the Ali-Bodmer partial-wave potential[29]:

$$V^{AB} = \sum_{l=0,2,4} V_l^{AB} \left|l\right\rangle \left\langle l\right| \tag{3.70}$$

with V_l^{AB} being

$$V_l^{AB}(r) = V_{r,l} e^{-\mu_r^2 r^2} - V_a e^{-\mu_a^2 r^2} \tag{3.71}$$

for the coordinate space case and

$$V_l^{AB}(p) = \frac{V_{r,l}}{8(\pi\mu_r)^{\frac{3}{2}}} e^{-\frac{(p-p')^2}{4\mu_r^2}} - \frac{V_a}{8(\pi\mu_a)^{\frac{3}{2}}} e^{-\frac{(p-p')^2}{4\mu_a^2}} \tag{3.72}$$

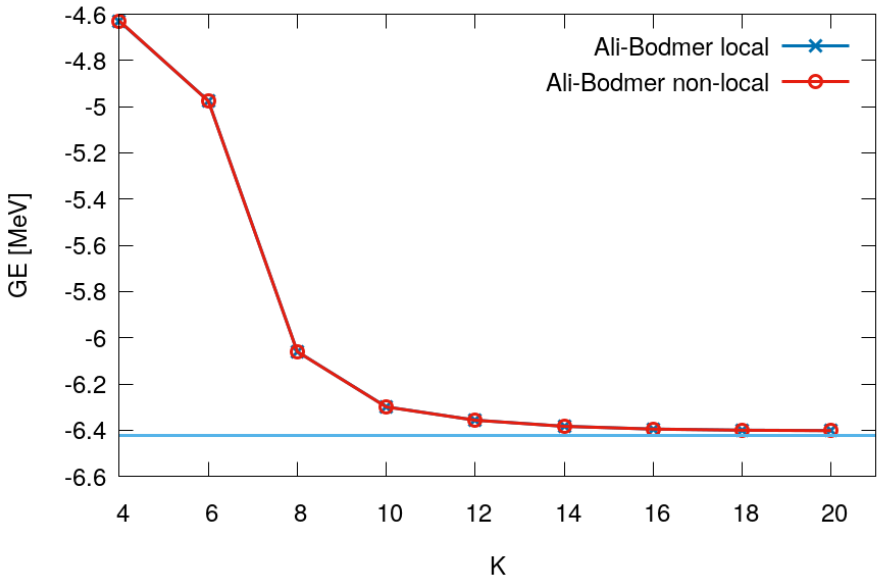

Figure 3.4: Comparison between the calculations of the ground state of Carbon-12 with an Ali-Bodmer interaction and its momentum space counterpart.

for the momentum space form.

The constants V_i and μ_i are $V_{r,0} = 500$ MeV, $V_{r,2} = 340$ MeV, $V_{r,4=10}$ MeV, $V_a = 130$ MeV, $\mu_r = 0.7$ fm^{-1} and $\mu_a = 0.475$ fm^{-1}.

The results of the calculation are shown in figure 3.4. As one can see, there is a perfect correspondence between the two spaces after the system becomes bound (at $K = 4$), with a difference between the two results of 400 eV at $K = 20$ over more than 6 MeV, less than a a part in ten thousand, showing the goodness of the program even when using systems composed of particles with different masses from the reference one, $m = m_{nucleon}$. In addition, as one can see, both results are also converging to the value of -6.2285 MeV calculated in the original paper[29].

Another test has been developed with the use of the same Ali-Bodmer potential together with a Coulomb repulsion, on the same Carbon-12 nucleus system. However, differently from the Helium case, there is the addition of a cutoff term $\mathrm{erf}(\beta r)$, giving to the Coulomb potential the following form in coordinate space:

$$V_C(r) = \frac{4e^2\,\mathrm{erf}(\beta r)}{r}. \tag{3.73}$$

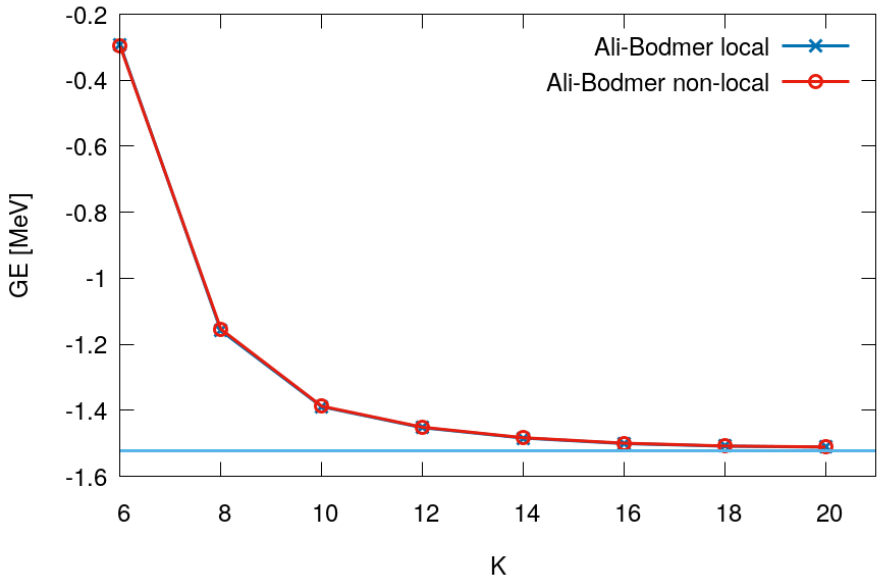

Figure 3.5: Comparison between the calculations of the ground state of Carbon-12 with an Ali-Bodmer+Coulomb interaction and its momentum space counterpart.

This potential can be also transformed in momentum space, where the error function becomes a Gaussian regulator

$$\frac{\mathrm{erf}(\beta r)}{r} \xrightarrow{\text{F.T.}} \frac{1}{2\pi(p-p')^2} e^{-\frac{(p-p')^2}{4\beta^2}}, \tag{3.74}$$

giving the final form to the potential in momentum space as

$$V_C(p,p') = \frac{4e^2}{2\pi(p-p')^2} e^{-\frac{(p-p')^2}{4\beta^2}}. \tag{3.75}$$

For the parameter β it was chosen the value $\sqrt{3}/2.88$ from the reference paper.
The results of the calculation of the ground state for the Carbon-12 nucleus are shown in figure 3.5.
As one can see, the addition of the Coulomb interaction adds, like it was shown in the case of the Minnesota potential in the ^{3}He system, a more serious divergence to be taken care of in momentum space than the correspondent divergence in real space. Such a divergence slows down the convergence in the non-local, momentum case, up to the point where it required, like in the previous cases, to reach 500 points in the Laguerre grid to obtain the same result between the two spaces. Still, as the figure shows, there is a good agreement between the two results, with differences in the final energies of less than a single keV, less than one part in a thousand.

Making a direct comparison with the results of the paper where this potential was introduced can also confirm the goodness of the obtained energies, since the authors of [29] obtained an energy of 1.523 MeV, comparable to the result of 1.511 MeV of this work.

The last benchmark needed for the program is the case of Beryllium-9. Differently from the previous systems analyzed in this section, the Beryllium nucleus presents, as the little figure 3.6 shows, a cluster nucleus (a definition that will be explained in the next chapter) configuration, a mix of two types of particles, neutrons and α-particles, different in both weight, charge and statistics: being the former particle a fermion and a nucleon (with both spin and isospin equal to 1/2), and the latter being a boson (with both spin and isospin equal to 0).

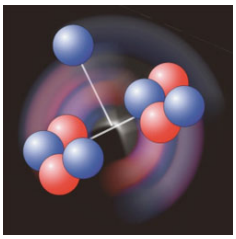

Figure 3.6: Schematic of a Beryllium-9 nucleus (P. Mueller/Argonne National Lab).

The construction of a new set of Jacobi coordinates for this new couple is not a problem, thanks to the reference mass reducing the difference with the previous ones to a single variable. However, while the $\alpha\alpha$ and nn couples are made of two identical particles, interacting through a nuclear potential (and a Coulomb potential too in the $\alpha\alpha$ case), the αn couple is between an electrically charged boson and an electrically neutral fermion, meaning that the Coulomb force between the two is zero and, different from the fermion-fermion and boson-boson couples that presented a natural antisymmetry and symmetry respectively, this new couple doesn't have a defined symmetry.

Calculating the ground state energy of a Beryllium-9 nucleus then becomes a much more difficult task, from a programming point of view, compared to the Carbon-12 nucleus. Every couple needs a special spin and isospin statistic and mass parameter tailored to itself before being used for the calculation of the final Hamiltonian matrix of the system and the basis states has to take into consideration the spin 1/2 states for the couple while, in the previous benchmarks used until now, it cared about only spin 0 and spin 1 states.

However, these necessary modifications have been accomplished with an high degree of success, obtaining an evolved program able to calculate the matrix elements in couples of bosons, fermions and mixed bosons and fermions, in momentum and coordinate space both with local and nonlocal potentials.

As the last test for the compatibility between the two spaces for this last case the first idea was using the Ali-Bodmer interaction as a "fake" interaction be-

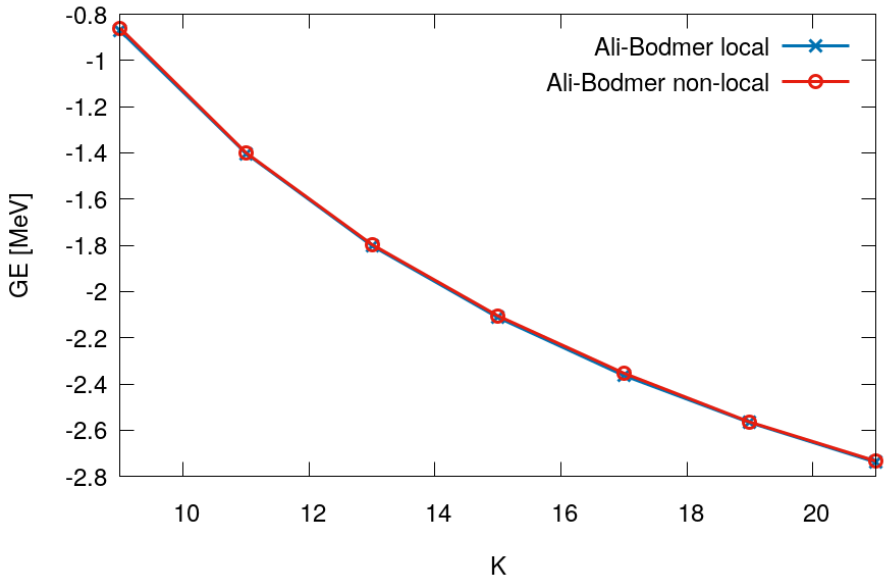

Figure 3.7: Comparison between the calculations of the ground state of Beryllium-9 with a modified Ali-Bodmer+Coulomb interaction and its momentum space counterpart.

tween α particles and neutrons, other than in $\alpha\alpha$ couples. However this lead to an unbound system. So the term V_a in the Ali-Bodmer potential (Eq. (3.72)) was modified, increasing it to 180 MeV, and resulting in a bound system, in both cases, coordinate space local potential and momentum space local potential. As in the case of Carbon-12 and the other nuclei there was a very good (roughly one part in a thousand) correspondence between the two cases, as can be seen from figure 3.7.

Chapter 4

Effective Field Theory

Contents

As described in the introduction my aim is the calculation of ^{9} Be in an $\alpha\alpha n$ cluster model, where the $\alpha - \alpha$ and $\alpha - n$ potentials are derived from an Effective Field Theory (EFT).
Therefore, in this chapter, I first want to give an introduction to Effective Theory. In addition I will present a brief outline of the historical development of cluster models in nuclear physics. Finally, I then come to the description of the $\alpha - \alpha$ and $\alpha - n$ EFT potentials, which had been derived in the master thesis of C.A. Manzata [30].

4.1 What is an Effective Theory?

Before moving towards the explanation of what EFT means, one has to understand what is an effective theory in general.

It is commonly known what Newtonian mechanics, called also classical mechanics, is, and how it can describe with quite a good precision the motion of macroscopic objects, be it a car or a planet. However, it is also known that, at much larger (and smaller) distances and energies than the one usually experienced in day-to-day life, classical mechanics makes poor predictions of objects' motion, with substantial deviations from the observations.
In these cases other theories, like quantum mechanics and relativity, can be used to make better predictions. In the realm of classical mechanics then these theories, in their approximate form, return to the original Newtonian formulation. We can see then that Newtonian mechanics takes the role of what is called an effective theory: a theory that has validity only in a certain regime of parameters or in certain length scales. As one moves outside of these limits the predictions given by the effective theory become less and less correct, moving away from the observed values. Then another theory can take its place, effectively creating a chain of effective theories, each one becoming more and more "fundamental" of the former, able to predict a larger and larger number of events and observations.
This does not mean that, once one has found a "more fundamental" theory than another, we have to abandon the latter. This effective theory indeed can still be used to make predictions in its range of validity. Not only this, in some cases the computational complexity of making calculations with a certain theory can exceed the capacity, in both time and computational power, at our disposal. Then an effective theory is not only a possibility, but a necessity. The use of an effective theory becomes then a powerful technique to make predictions and to validate the underlying theories used to build it. This is the case that brought the creation of the so-called Effective Field Theories (EFTs). Such theories have been generated from studies of QCD and QED, where it exists a 'range', beyond which increasingly complex problems arise. For example, the QCD theory beyond the size of a nucleon loses its perturbative nature, the QED theory gets increasingly complex as the range in which interactions are studied diminishes. The idea is then to hide all this complexity for the calculation of low-energy states, by treating this complicated interaction as perturbative for the long-range behaviour. Ignoring the substructures, the short-range mechanisms and degrees of freedom, one then is able to study systems that would have been too complex before, allowing the testing of theories on new structures.
In order to understand better how an effective field theory in the case of this thesis, cluster nuclei, is implemented, I will show some common techniques for the creation of effective theories.

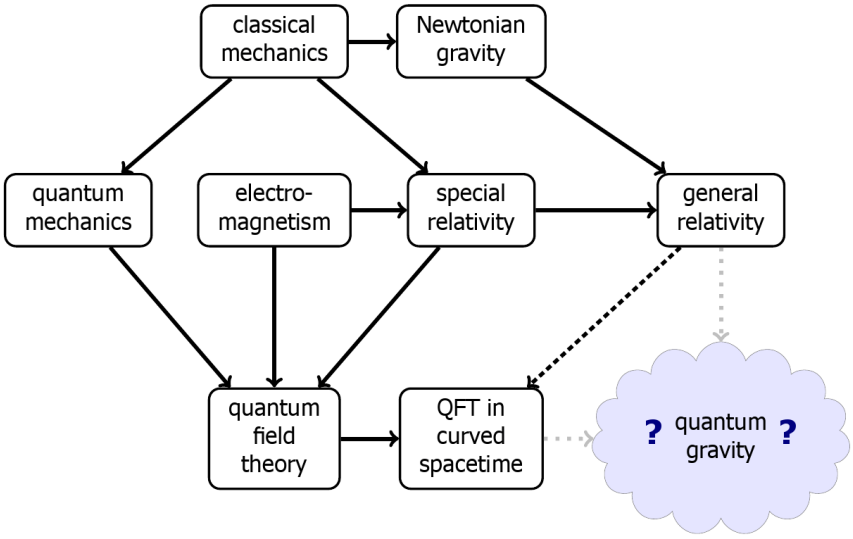

Figure 4.1: A scheme of the relation between theories in Physics. Starting from classical Mechanics and adding quantization, limited speed of light and/or gravity, one can move toward more fundamental and complete theories.

4.1.1 Multipole expansion

A very common technique in the construction of the Effective Theories, and also one of the first a student in Physics meets, is the multipole expansion.
While comparatively simpler than most of other methods, it shows to great effect the basis of this type of techniques.
The basic idea is to apply a Taylor expansion on an arbitrary function (that will be our potential) $V(\boldsymbol{r}-\boldsymbol{R})$ around the origin $\boldsymbol{r}=0$:

$$V(\boldsymbol{r}-\boldsymbol{R}) = V(\boldsymbol{R}) - \sum_{\alpha=x,y,z} r_\alpha V_\alpha(\boldsymbol{R}) + \frac{1}{2}\sum_{\alpha,\beta=x,y,z} r_\alpha r_\beta V_{\alpha,\beta}(\boldsymbol{R}) + ... \tag{4.1}$$

where

$$V_\alpha(\boldsymbol{R}) = \left(\frac{\partial V(\boldsymbol{r}-\boldsymbol{R})}{\partial r_\alpha}\right)_{\boldsymbol{r}=0} \text{ and } V_{\alpha,\beta}(\boldsymbol{R}) = \left(\frac{\partial^2 V(\boldsymbol{r}-\boldsymbol{R})}{\partial r_\alpha . \partial r_\beta}\right)_{\boldsymbol{r}=0} \tag{4.2}$$

The most common example is the case of the Coulomb potential of a distribution of point charges at a distance $\boldsymbol{R} \gg \boldsymbol{r}_i$, with $\boldsymbol{r}_i$ the position vector of the single charges q_i:

$$V(\boldsymbol{R}) = \sum_{i=1}^{N} \frac{q_i}{|\boldsymbol{r}_i - \boldsymbol{R}|} = \frac{q}{R} + \frac{1}{R^3}\sum_{\alpha=x,y,z} P_\alpha R_\alpha + \frac{1}{2R^5}\sum_{\alpha,\beta=x,y,z} Q_{\alpha,\beta} R_\alpha R_\beta + ... \tag{4.3}$$

where we see the first three terms of such an expansion, the monopole term with $q = \sum_{i=1}^{N} q_i$, the dipole one with $P_\alpha = \sum_{i=1}^{N} q_i r_{i,\alpha}$ and the quadrupole one with $Q_{\alpha,\beta} = \sum_{i=1}^{N} q_i(3r_{i,\alpha}r_{i,\beta} - \delta_{\alpha\beta}r_i^2)$.
As one can see, the terms become smaller and smaller as they go on, but only in the case $\boldsymbol{R} \gg \boldsymbol{r}_i$.
This shows what has been said before: one can take a complicated interaction, like the one between many point charges, and move it to a simpler form (a monopole interaction), with smaller and smaller corrective terms (the dipole and quadrupole and other, higher order, terms) in a limited range (in this case as $\boldsymbol{R}$ remains large compared to the various $\boldsymbol{r}_i$).

4.1.2 Earth's gravitational potential

Another common subject of Physics students is the gravitational acceleration exerted by our planet. As it is commonly known, such a quantity in Newtonian physics is $g = GM/R^2$ (with M the mass of the Earth and R it's radius). Also it is well-known that, for an object of mass m moving at a height h from the surface of Earth, the gravitational potential is given by

$$\Delta U = mgh. \tag{4.4}$$

This is also an effective theory, since the expression above is just an approximation of

$$\Delta U = \frac{GMm}{r_i} - \frac{GMm}{r_f}. \tag{4.5}$$

Indeed, giving an initial distance $r_i = R$ and as the final distance $r_f = R + h$, in the limit $h \ll R$ one can expand the formula in Eq. (4.5) as

$$\Delta U = \frac{GMm}{R} - \frac{GMm}{R+h} = \frac{GMm}{R}\frac{h}{R+h} = \tag{4.6}$$

$$= \frac{GM}{R^2}mh\frac{R}{R+h} = mgh\frac{R}{R+h}, \tag{4.7}$$

and, expanding over $h/R \ll 1$, we obtain

$$\Delta U = mgh\left(1 - \frac{h}{R} + \frac{h^2}{R^2} + ...\right). \tag{4.8}$$

Taking the first term of this expansion (a term much bigger than the others, in the limit we are considering) we obtain the first result.
As one can see, this is another example of an Effective Theory. Even more clearly than the multipole expansion, we can easily see that there is only a certain maximum range under which this theory works, the distance R. Indeed, above

such a limit the expanded formula doesn't even converge anymore, marking this a hard limit to our theory. This distance, this extreme limit to our effective theory, is called the breakdown scale.
Also we can observe another essential mechanism of this type of effective theories and that is, the control over the error. Every term in the potential energy after the first one becomes dependent on a progressively higher power of h/R. This means two very important things. First and foremost, while it is true that adding terms to our potential will increase the quality of our prediction, the correction to the final energy will become progressively smaller. On the other side, the error will proportionally get smaller as well. The addition of terms is the addition of computational load as well, so when developing such an effective theory one needs to find a balance between the benefits of adding terms to the effective potential (better prediction, smaller errors) and the disadvantages (increased computational complexity and load for smaller and smaller corrections).

4.1.3 Schrödinger equation

While these examples were useful in understanding what is an Effective Theory, they are still applied on relatively simple problems, enough that we could technically still calculate the full problem. However, there are problems where the behaviour at certain scales becomes much more complicated, enough that sometimes an Effective Theory is not a preferred but also the only way one can proceed.
The bulk of Effective Theory is based on a simple principle: the low-energy (long range) physics is insensitive to the details of the high-energy (short range) one. We can then control and contain the high-energy physics, putting in a simple expression its effects on the long-range behaviour. Lepage [7], wrote a quite complete discussion of this procedure, which will be briefly summed up in this section. In short, the steps to make an Effective theory are the following:

1. Introduce a scale that separates low-energy (long range) and high-energy (short range) physics.

2. Find and describe the low-energy behaviour of the theory.

3. Introduce a cutoff in order to exclude the short range behaviour.

4. Add a finite number of local correction terms to the effective Hamiltonian, which should describe the effects of the short range physics in the long range one.

5. Fit the corresponding parameters to the experimental data.

Lepage applied this process to a quantum system, consisting in a particle of mass m interacting through a Coulomb potential plus a short-range, 'nuclear-like' potential $V_s(\boldsymbol{r})$:

$$H = T + V = \frac{p^2}{2m} - \frac{\alpha}{r} + V_s(\boldsymbol{r}). \tag{4.9}$$

Following the aforementioned steps, one must first identify the low-energy behaviour. In this quite simple example one can see that at a long-range in the effective potential one should obtain the Coulomb interaction. Then one needs to regularize such an effective potential, adding a cutoff. To obtain such a result, we can move in momentum space, adding a Gaussian regulator:

$$\frac{\alpha}{r} \to \frac{4\pi}{q^2} e^{-q^2 a^2/2} \tag{4.10}$$

where q is the exchanged momentum and $\Lambda = 1/a$ is our cutoff.
As one can see, as q increases our potential fall off to zero, thereby excluding the high-energy, short-range ($< \Lambda$) terms, reaching zero in the limit $r = 0 \Leftrightarrow q \to \infty$, and therefore regularizing our interaction.
The next step in the creation of this effective potential is returning to coordinate space, through the inverse Fourier transform, the form of which was seen in the third chapter:

$$\frac{\mathrm{erf}(r/\sqrt{2}a)}{r}, \tag{4.11}$$

where

$$\mathrm{erf}(x) = \frac{2}{\pi} \int_0^x e^{-t^2} dt \tag{4.12}$$

is the error function.
To this potential one needs to add the short range interaction, so we will mimic it through correction terms. The low-momentum behavior of any short-range potential is efficiently described in terms of the Taylor expansion in momentum space. Transforming back to coordinate space gives a series that is a polynomial in the momentum operator $\boldsymbol{p} = -i\nabla$ multiplied by a delta function. In order to avoid infinities we need to introduce an ultraviolet cutoff, therefore we smear the delta function over a volume whose radius is approximately our cutoff distance a. Then a good choice, useful for avoiding infinities, is the use of the smeared three-dimensional delta function and its derivatives:

$$\delta_a^3(\boldsymbol{r}) = \frac{e^{-r^2/2a^2}}{(2\pi)^{3/2} a^3}, \tag{4.13}$$

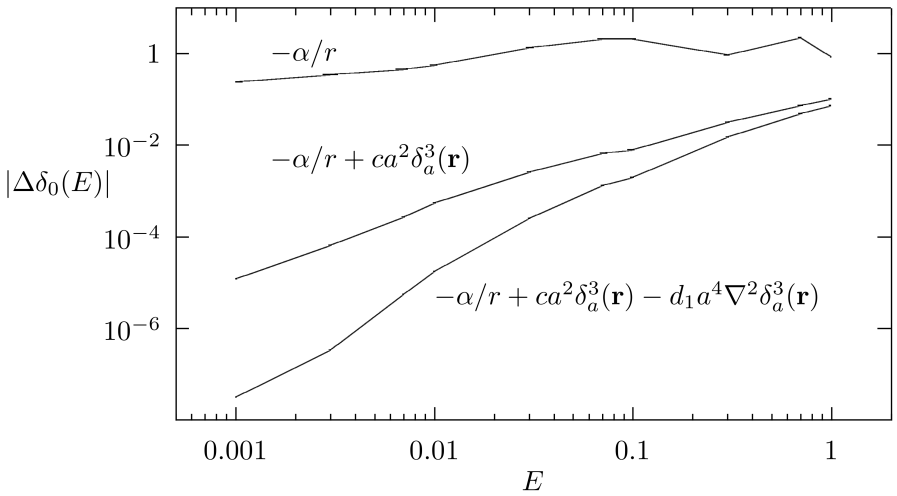

Figure 4.2: S-wave phase shifts errors for the non-corrected interaction and for the corrected ones, both with only a^2 terms and with also a^4 terms. Example from Lepage [7] paper.

giving to our effective potential its final form:

$$V_{eff}(\boldsymbol{r}) = -\frac{\alpha}{r}\,\mathrm{erf}(r/\sqrt{2}a) + ca^2\delta_a^3(\boldsymbol{r}) + d_1a^4\nabla^2\delta_a^3(\boldsymbol{r}) + d_2a^4\nabla\cdot\delta_a^3(\boldsymbol{r})\nabla + ... \tag{4.14}$$

As seen in Fig. 4.2, where it is shown the error on the phase shifts compared to the complete potential (after determining the value of the constants c and d on a set of synthetic data), one can easily see the improvement brought by the effective potential even at lower orders, compared to only the Coulomb potential. At low energies (measured in a^2m), the errors decrease steadily as the correction terms are added, order-by-order in a^2. The slope of the error curve changes as each new correction is added, getting steeper by one power of $E \propto p^2$ each time the order of the error is increased by a^2. At values of $E > 1$ the particle wavelength is short enough that it is able to probe the details structure of the short range potential $V_s(\boldsymbol{r})$, putting a limit on where our effective potential can be used.

4.1.4 Fermi electroweak interaction

Last in this series of examples, I will show a historical use of effective potential in quantum field theory, that is, an Effective Field Theory.
In 1933, before the development of the Standard Model, Wolfgang Pauli proposed a theory in order to explain the peculiar characteristics of the β decay,

namely the continuous energy spectrum and the apparent lack of conservation of angular momentum. In this theory Pauli hypothesized the existence of another, very small neutral particle, the neutrino, while Enrico Fermi developed quite a peculiar Lagrangian for the particles involved to interact with. While, as of today, we know that the β decay is quite different from what Fermi imagined, such a theory was an important milestone in the road toward the Standard model. Not only, such a theory was in reality an effective theory of the real one, as I will show in this section.
Fermi proposed a pointlike interaction described by the following Lagrangian:

$$\mathcal{L}(x) = \frac{G_F}{\sqrt{2}} V_\mu^\dagger(x) V'^\mu(x), \tag{4.15}$$

with V_μ as a vector current and G_F as the Fermi constant, known today to fulfill the following relations

$$G_F = \frac{\sqrt{2}g^2}{8M_W^2} \simeq 1.1663787(6) \times 10^{-5} GeV^{-2} \tag{4.16}$$

and g is the coupling constant of the weak interaction. Taking into account parity violation Sudarshan and Marshak, Feynman and Gell-Mann and Sakurai in 1957 rewrote the previous Lagrangian [31] as

$$\mathcal{L}(x) = \frac{G_F}{\sqrt{2}} (V_\mu^\dagger - A_\mu^\dagger)(V'^\mu - A'^\mu), \tag{4.17}$$

where A_μ is a vector-axial current.
We now know that the β^- decay is mediated by the W^- boson, which gives the following modification to the amplitude:

$$\frac{G_F}{\sqrt{2}} (V_\mu^\dagger - A_\mu^\dagger)(V'^\mu - A'^\mu) \to \frac{G_F}{\sqrt{2}} (V_\mu^\dagger - A_\mu^\dagger) P_{\mu\nu} (V'^\nu - A'^\nu), \tag{4.18}$$

where

$$P_{\mu\nu} = \frac{-g_{\mu\nu} + q_\mu q_\nu / M_W^2}{q^2 - M_W^2}, \tag{4.19}$$

with q_μ and M_W as the four-momentum and mass of the W boson, respectively.
Moving in the limit $q^2 \ll M_W^2$ one has $P_{\mu\nu}$ equal to

$$\frac{g_{\mu\nu}}{M_W^2}, \tag{4.20}$$

meaning that both theories lead to the same low-energy result. One can then see that the modified Fermi interaction is an Effective Field Theory ante-litteram, one of the first examples. Not only that, it is also an example of how good in their range of validity such theories can be. Being the mass of the W^- boson

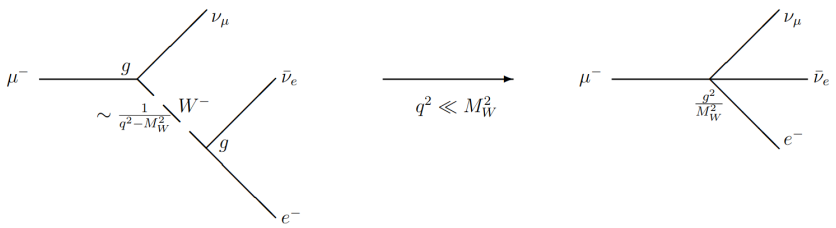

Figure 4.3: The Fermi diagram of the muon decay, mediated through the weak force and the 'Fermi-theory like' diagram one gets at a low-momenta approximation.

around 80 GeV and the first experiments in the tens of MeV, it was quite some time before the modified Fermi theory could be experimentally shown to be not complete. This was quite the problem at the time, because calculations had shown that the Fermi theory of weak interactions is not renormalizable.

4.2 Effective theory in cluster nuclei

As shown in [7] in the previous examples, in order to create an effective potential, an effective interaction that can predict low-energy levels of a system as well as the more "fundamental" and complicated interactions can, one needs a separation of scales, a possibility to "hide" the high-energy structure inside a certain range, a cutoff.

4.2.1 A brief history of cluster nuclei

Since the beginning of nuclear studies it was known, in Nature particles like to aggregate together. From nuclei and electrons to atoms, from atoms to molecules to crystalline structures, the elementary particles at a certain length (and energy) scale create the ones at the next level. And the same happens inside the nucleus. Moving from quarks and gluons to the quark triplets that compose nucleons, to the nucleons themselves, one can move from a scale of energy to another. And in some peculiar nuclei the process continues, with particles aggregating in certain substructures that finally compose the nucleus. These are called halo and cluster nuclei.

In order to minimize the repulsion due to Pauli exclusion principle nucleons will try to pair with spin anti-aligned and in orbitals with maximal overlap, leaving a spin-zero entity. Of course, it is possible for both pairs of protons and neutrons to perform this same pairing, resulting in a maximally correlated quartet of two protons and two nucleons known as the α-particle. This correlation gives

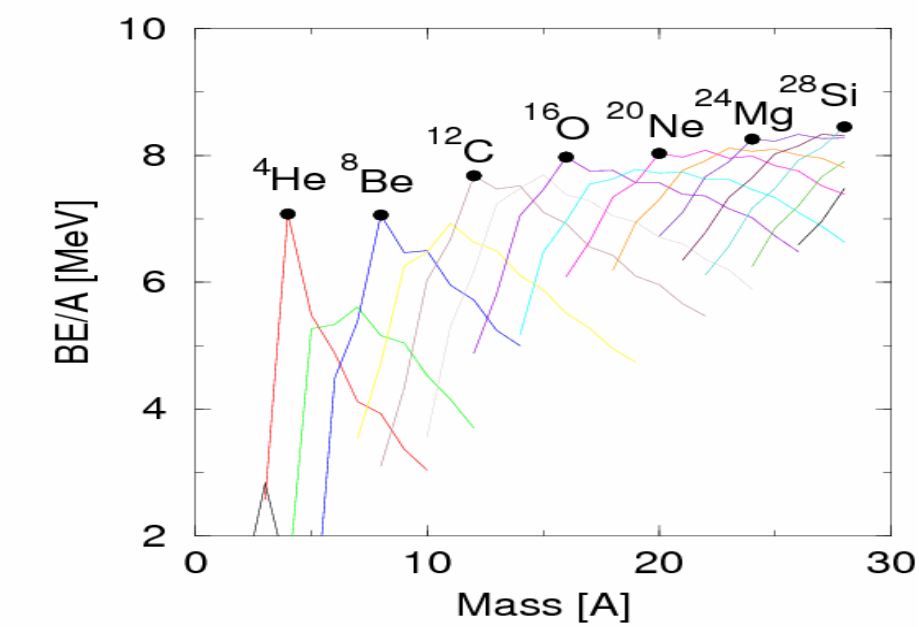

Figure 4.4: Binding energy per nucleon of light nuclear systems (up to $A = 28$), the lines connect isotopes of each element. The α-particle nuclei are marked by the circles.

the α-particle one of the highest binding energies per nucleon amongst all light nuclei. Usually a bound nucleon possesses a binding energy of the order of 8 MeV. The α-particle's first excited state excitation energy is at a much higher value of 20 MeV, suggesting that the α-particle bound system is a natural state for nucleons in a nucleus to fall in. This initial idea is further strengthened by ab-initio calculations of light nuclei where this type of alpha-clustering seems to be a preferred configuration [32]. Other studies [33] have shown that the nuclear surface plays a critical role in the formation of clusters. When the nuclear density falls to one third of normal nuclear matter density, there is expected to be a phase change and nucleons condense into α-particles. So there is a strong theoretical evidence that nucleons prefer to aggregate together in nuclear substructures, mainly α-particles, inside light nuclei. This type of nuclei are called cluster nuclei. The only question that remains is this clustering effect is effectively real, or it is just a bizarre flaw of the theory.

Since the discovery of the phenomenon of α decay in heavy nuclei, the idea that protons and neutrons could form together an α substructure gained traction in the scientific community.

As one can see from Fig. 4.4, analyzing the binding energies per nucleon of the

light nuclei one can find that the nuclei with even and equal number of nucleons and protons (^{4}He, ^{8}Be, ^{12}C, ^{16}O...) have the highest binding energy per nucleon among all the isotopes of said nucleus and among all nuclei close in atomic number. These nuclei have been called α-conjugate nuclei, since their peculiar atomic number $A = 4n(n = 2, 3, 4, ...)$ and number of neutrons $N = Z$ allows them to be entirely made of α particles.

These systems were examined more in depth in 1938 in an important paper by Hafstad and Teller [8], who charted the evolution of the binding energy with number of 'bonds' or connections between the α-particles (figure 4.5). The seemingly linear relationship pointed to an apparently constant $\alpha-\alpha$ interaction and also to the resilience of the α-particles in the ground states of these nuclei.

In the 1960s it was understood that, in order to be fully formed the proximity of cluster states to the decay threshold is crucial. This has become encapsulated in what is known as the Ikeda diagram [34](figure 4.6). This would predict that cluster structures are most obvious at an excitation which coincides with a par-

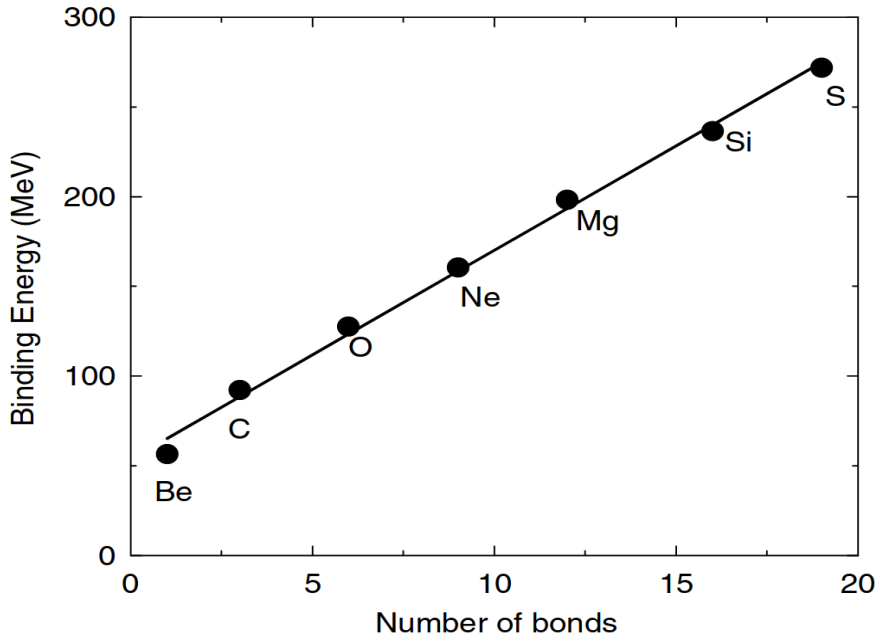

Figure 4.5: Binding energy per nucleon of $A = 4n$ nuclei versus the number of $\alpha - \alpha$ bonds. The analysis by Hafstad and Teller [8] suggested that the ground states of $A = 4n$, α-conjugate, nuclei could be described by a constant interaction energy scaled by the number of bonds. For ^{8}Be there is one bond, for ^{12}C three, six for ^{16}O, nine for ^{20}Ne, twelve for ^{24}Mg and for structural reasons (the geometric packing of the α-particles) sixteen for ^{28}Si.

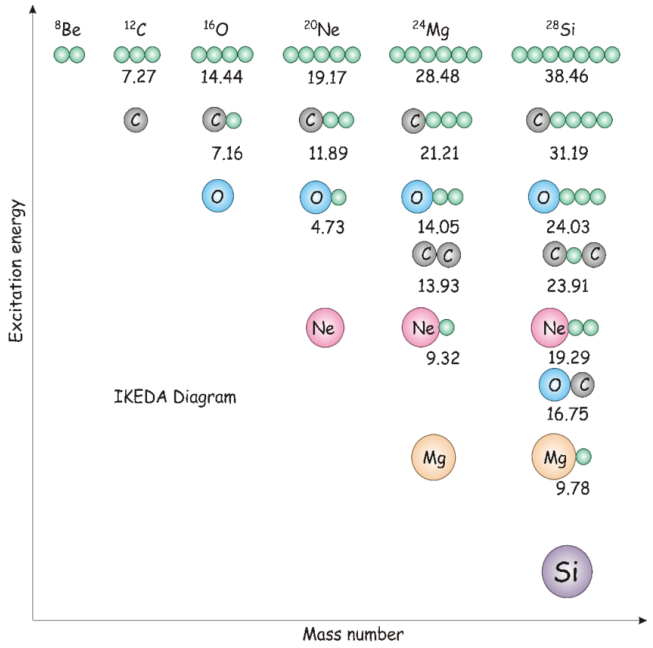

Figure 4.6: The Ikeda diagram. The threshold energies for each configuration are given in MeV. The smallest, unlabelled clusters are alpha particles. Increasing excitation energy is required to form more and more complex cluster structures. Figure from [9]

ticular decay threshold. Hence, the $\alpha + \alpha$ cluster structure found in the ground state of ^{8}Be (which undergoes α-decay with an half-life of $6.7(17) \times 10^{-17}$ s). The three alpha-cluster structure would be expected to be close to the three alpha-decay threshold (7.3367 MeV). Indeed there is such an excited state in Carbon-12, the famous state predicted by Fred Hoyle in 1954 [35]. The excited Hoyle state of ^{12}C is 7.656 MeV above the ground state, allowing the aforementioned three-α process that leads to the abundant carbon in the Universe.

The research on alpha-clustered nuclei, especially the lighter ones like Beryllium-8 and Carbon-12, continued in the following years.

The simplest case is that of the two α-particle system, the Beryllium-8 nucleus. The single α-particles in this resonance are tightly bounded by themselves, creating a peculiar dumbbell-like structure that gives rise to a rotational band, from which the moment of inertia is found to be commensurate with an axial deformation of 2:1. The binding energy of the α-particle is so large that even systems close in atomic number such as ^{6}Li and ^{7}Li display visible cluster structures ($\alpha + d$ and $\alpha + t$ respectively).

In 1957 it was found experimental evidence of the predicted Hoyle state [36],

and a 100 keV resonance in ^{24}Mg, discovered in the 1960s, was later interpreted as a ^{12}C+^{12}C cluster state.
Even more experimental evidences for the cluster structure of light nuclei have been found and they are well documented (see [37] and references therein).
To this day several nuclei have been recognized as being cluster nuclei, among which the aforementioned Beryllium-9 and Carbon-12. In these nuclei one then can recognize the presence of a natural separation of scales, the necessary requirement for the creation of an Effective Field Theory potential.

4.2.2 Partial wave decomposition

The interaction between α clusters and neutrons inside of a ^{9}Be nucleus is very weak, especially compared to the one holding the α-particles together. Indeed, it's so weak that the two types of subsystems of ^{9}Be, the $\alpha\alpha$ pair and the αn one, alone don't give rise to a bound state. The bound state in Beryllium-9 and Carbon-12 nuclei is purely due to a three-body phenomenon. These types of systems are called Borromean (after the name Borromean rings, a system composed by three rings, in which, removing any of them, the remaining two are left unlinked).
To give a quantitative value to this "weak link" between clusters and neutrons, one can remember that the binding energy per nucleon of ^{9}Be nucleus is 6.463 MeV, meaning that the total binding is

$$\text{BE}(^9\text{Be})=58.164 \text{ MeV}. \tag{4.21}$$

Removing the internal binding energy of the two α-particles one gets an effective binding energy of

$$\text{B}_3(^9\text{Be})=\text{BE}(^9\text{Be})\text{-}2\text{BE}(\alpha)=1.572 \text{ MeV}, \tag{4.22}$$

well below the break-up threshold of the α-particle into ^{3}H+p, the proton separation energy

$$\text{S}_p(^4\text{He})=19.813 \text{ MeV}. \tag{4.23}$$

Since $\text{B}_3(^9\text{Be}) \ll \text{S}_p(^4\text{He})$, the dynamics describing the clustering configuration of ^{9}Be can be considered insensitive to the internal dynamics of α. Therefore one can treat α as a point particle and introduce contact interactions between $\alpha\alpha$ and αn, described as a in Fig. 4.7.
At low energies, one can describe the contact potential as

$$\langle \boldsymbol{x}| \, V(\boldsymbol{x}) \, |\boldsymbol{x}\rangle = (2\pi)^3[\lambda_0 - \lambda_1(\nabla^2 + \nabla'^2)]\delta^{(3)}(\boldsymbol{x}-\boldsymbol{x}')\delta^{(3)}(\boldsymbol{x}) \tag{4.24}$$

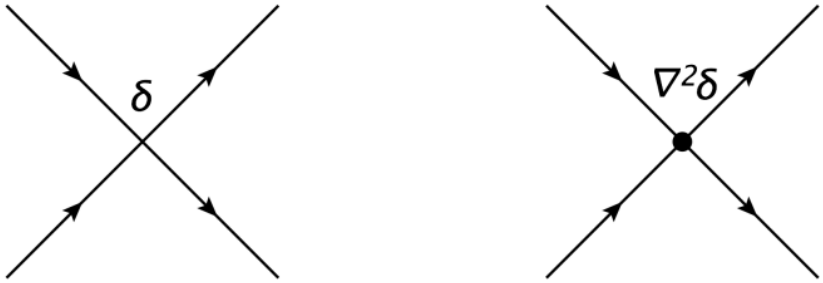

Figure 4.7: Feynman diagrams for a contact interaction, described as a delta function and its derivative.

Here I will use the Fourier transform of this potential, a non-local interaction which has a separable form:

$$V(\boldsymbol{p},\boldsymbol{p}') = \lambda_0 + \lambda_1(p^2 + p'^2), \tag{4.25}$$

where p and p' are the two-body relative momenta. This can be rewritten in the compact form

$$V(\boldsymbol{p},\boldsymbol{p}') = \sum_{i,j=0}^{1} p^{2i}\lambda_{ij}p'^{2j}, \tag{4.26}$$

where we have introduced the matrix

$$\lambda = \begin{pmatrix} \lambda_0 & 0 \\ 0 & \lambda_1 \end{pmatrix}. \tag{4.27}$$

As seen in [38] we can, in general, expand a potential in partial-wave components by defining

$$V_l(p,p') = \frac{1}{2}\int_{-1}^{1} \langle \boldsymbol{p}| V |\boldsymbol{p}'\rangle \, P_l(\hat{\boldsymbol{p}}\cdot\hat{\boldsymbol{p}}')d(\hat{\boldsymbol{p}}\cdot\hat{\boldsymbol{p}}'), \tag{4.28}$$

$$V(\boldsymbol{p},\boldsymbol{p}') = \langle \boldsymbol{p}| V |\boldsymbol{p}'\rangle = \sum_{l=0}^{\infty}(2l+1)V_l(p,p')P_l(\hat{\boldsymbol{p}}\cdot\hat{\boldsymbol{p}}'), \tag{4.29}$$

where P_l is the l-th Legendre polynomial. In particular, for a potential dominated by a specific partial wave l

$$V(\boldsymbol{p},\boldsymbol{p}') = p^l p'^l g(p)g(p') \sum_{i,j=0}^{1} p^{2i}\lambda_{ij}p'^{2j}(2l+1)P_l(\hat{\boldsymbol{p}}\cdot\hat{\boldsymbol{p}}') \tag{4.30}$$

where the λ matrix is defined as in (4.27). $V(\boldsymbol{p},\boldsymbol{p}')$ is modified by introducing the regulator $g(p)$, which regulates the short-distance dependence of the interaction, such that

$$g(p=0) = 1 \text{ and } g(p\to\infty) = 0. \tag{4.31}$$

The two indices i and j, in principle, could be larger than 1, but we are limiting them in order to get a phase shift expansion up to the effective range order, being for the on-shell T-matrix

$$\frac{k^{2l+1}}{T_l^{on}(E)} = -\frac{\mu}{2\pi}\left(\frac{1}{\alpha_l} + \frac{1}{2}r_{e,l}k^2 - ik^{2l+1}\right) + o(k^3) \tag{4.32}$$

with the scattering parameters being the scattering length α_l and the effective range $r_{e,l}$.

The partial wave expansion shown here is important in the study of Beryllium-9 and Carbon-12 nuclei, for two reasons. First, the two possible interactions (between α-particles and between alphas and neutrons) have a particularly predominant wave. The $\alpha\alpha$ interaction is dominated by the $^1S_0$ state, the ^{8}Be resonance, while the αn interaction has a resonance in the $^2P_{3/2}$ one. The second reason will be explained further in this thesis, when Euler angles will be introduced.

After this one needs to find an explicit expression for the coefficients λ_0 and λ_1 in terms of some experimentally measurable quantities (the scattering length and the effective range in this case) and with a dependence on a cutoff, that will be called Λ. The latter is necessary in this model for the presence of ultraviolet divergences, to give meaning to the potential in (4.24) and to absorb the regularization dependence of the predicted observables.

4.2.3 αn and $\alpha\alpha$ potentials[1]

The coefficients for the potential were found by expanding the Lippman-Schwinger equation in partial waves in a similar manner to (4.29):

$$T(\boldsymbol{p},\boldsymbol{p}') = \sum_{l=0}^{\infty}(2l+1)T_l(p,p')P_l(\hat{\boldsymbol{p}}\cdot\hat{\boldsymbol{p}}') \tag{4.33}$$

where

$$T_l(p,p') = p^l p'^l g(p)g(p')\sum_{i,j=0}^{1} p^{2i}\tau_{ij}(E)p'^{2j}. \tag{4.34}$$

What differs between the two cases is how the Lippman-Schwinger equation is generated. While in the case of the couple αn the Lippman-Schwinger equation takes the form

$$T(\boldsymbol{p},\boldsymbol{p}') = V(\boldsymbol{p},\boldsymbol{p}') + \int \frac{d\boldsymbol{q}}{(2\pi)^3}V(\boldsymbol{p},\boldsymbol{q})\frac{1}{E-\frac{q^2}{2\mu_{\alpha n}}+i\epsilon}T(\boldsymbol{q},\boldsymbol{p}') \tag{4.35}$$

[1] The following section therein shown is a small summary of the work made by C.A. Manzata in his master's thesis [30].

with $E = k^2/(2\mu_{\alpha n})$, while in the case of the $\alpha\alpha$ couple interaction one has to consider the presence of the Coulomb interaction, a long range interaction.
The presence of a potential at an infinite distance impacts on the in/out waves $\psi_{\boldsymbol{p}}^{(\pm)}$ used in the Lippman-Schwinger equation, distorting them

$$\left|\psi_{\boldsymbol{p}}^{(\pm)}\right\rangle = \left[1 + G_C^{(\pm)} V_C\right] |\boldsymbol{p}\rangle \tag{4.36}$$

where $G_C^{(\pm)}$ is the retarded/advanced Green's function in the case of a purely Coulomb interaction.
The T-matrix is now given by two contributions:

$$T(\boldsymbol{p}, \boldsymbol{p}') = T_C(\boldsymbol{p}, \boldsymbol{p}') + T_{SC}(\boldsymbol{p}, \boldsymbol{p}'), \tag{4.37}$$

where the pure Coulomb one is

$$T_C(\boldsymbol{p}, \boldsymbol{p}') = \langle \boldsymbol{p}' | \, V_S \left|\psi_{\boldsymbol{p}}^{(+)}\right\rangle \tag{4.38}$$

and the Coulomb-modified strong one is

$$T_{SC}(\boldsymbol{p}, \boldsymbol{p}') = \left\langle \psi_{\boldsymbol{p}}^{(-)} \right| V_S \left|\Psi_{\boldsymbol{p}}^{(+)}\right\rangle, \tag{4.39}$$

with

$$\left|\Psi_{\boldsymbol{p}}^{(\pm)}\right\rangle = \sum_{n=0}^{\infty} (G_C^{(\pm)} V_S)^n \left|\psi_{\boldsymbol{p}}^{(\pm)}\right\rangle = \left|\psi_{\boldsymbol{p}}^{(\pm)}\right\rangle + G_C^{(\pm)} V_S \left|\psi_{\boldsymbol{p}}^{(\pm)}\right\rangle \tag{4.40}$$

This modification applied to the Lippman-Schwinger equation results in the following expression for the strong force coupled with the Coulomb one:

$$\begin{aligned} T_{SC}(\boldsymbol{p}, \boldsymbol{p}') = &\left\langle \psi_{\boldsymbol{p}}^{(-)} \right| V_S \left|\psi_{\boldsymbol{p}}^{(+)}\right\rangle - \\ &- 2\mu_{\alpha\alpha} \int \frac{d\boldsymbol{p}''}{(2\pi)^3} \left\langle \psi_{\boldsymbol{p}'}^{(-)} \right| V_S G_C^{+} \left|\psi_{\boldsymbol{p}''}^{(-)}\right\rangle \frac{T_{SC}(\boldsymbol{p}, \boldsymbol{p}'')}{p^2 - k^2 + i\epsilon}. \end{aligned} \tag{4.41}$$

Following these definitions, the next step is putting the partial wave decomposition into the Lippman-Schwinger equations. This operation allows us to define the T-matrix τ_{ij} for the two possible cases. The next calculations, rather long and outside of the scope of this thesis, are well documented in [30]. In short, the resulting expressions are expanded in k^2/Λ^2 and evaluated for the relevant partial waves (S-wave for the $\alpha\alpha$ interaction and P-wave for the αn one). After the addition of the necessary cutoffs

$$\begin{cases} g(k)_{\alpha n} = e^{-(\frac{k}{\Lambda})^4} \\ g(k)_{\alpha\alpha} = \theta(k - \Lambda) \end{cases} \tag{4.42}$$

one will find two couples of equations that will give us λ_0 and λ_1. In the αn case solving such equations we get:

$$c_0 = \left[\frac{\left(\frac{f_{5,2}}{5} - \frac{1}{c_1}\right)^2}{\frac{f_{3,2}}{3} - \frac{\pi}{2a_1\Lambda^3}} - \frac{f_{7,2}}{7}\right] c_1^2 \tag{4.43}$$

$$c_1 = \frac{5}{f_{5,2}}\left\{1 \pm \left[1 - \frac{\left(f_{1,2} + \frac{r_1\pi}{4\Lambda}\right)\frac{f_{5,2}}{5}}{\left(\frac{f_{3,2}}{3} - \frac{\pi}{2a_1\Lambda^3}\right)^2}\right]^{-\frac{1}{2}}\right\} \tag{4.44}$$

where

$$\lambda_0 = -\frac{1}{8\pi\mu_{\alpha n}}\frac{c_0}{\Lambda^3} \tag{4.45}$$

$$\lambda_1 = -\frac{1}{8\pi\mu_{\alpha n}}\frac{c_1}{\Lambda^5}, \tag{4.46}$$

the function

$$f_{n,m} = \frac{n}{\Lambda^n}\int_0^\infty dq q^{n-1} e^{-2(\frac{q}{\Lambda})^2 m} = \left(\frac{1}{2}\right)^{\frac{n}{2m}}\Gamma\left(\frac{n}{2m} + 1\right) \tag{4.47}$$

and $a_1 = -62.951$ fm^3 and $r_1 = -0.8819$ fm^{-1} the scattering parameters (the scattering volume and effective range respectively).
In a similar manner one can find the equations connecting the scattering quantities $a_0 = -1920$ fm and $r_0 = 1.099$ fm to c_0 and c_1 for the $\alpha\alpha$ coupling:

$$\widetilde{c}_0 = \left[\frac{\left(\frac{f_3}{3} - \frac{1}{c_1}\right)^2}{f_1 - \frac{\pi}{2a_0\Lambda}} - \frac{f_5}{5}\right] c_1^2 \tag{4.48}$$

$$c_1 = \frac{3}{f_3}\left\{1 \pm \left[1 - \frac{\left(-f_{-1} + \frac{r_0\pi\Lambda}{4}\right)\frac{f_3}{3}}{\left(f_1 - \frac{\pi}{2a_1\Lambda}\right)^2}\right]^{-\frac{1}{2}}\right\} \tag{4.49}$$

where

$$\widetilde{\lambda}_0 = -\frac{1}{8\pi\mu_{\alpha\alpha}}\frac{\widetilde{c}_0}{\Lambda} \tag{4.50}$$

$$\widetilde{\lambda}_0 = \lambda_0 - \left(\frac{32\alpha\mu_{\alpha\alpha}}{\pi}\Lambda + 64\alpha^2\mu_{\alpha\alpha}^2\right)\lambda_1 \tag{4.51}$$

$$\lambda_1 = -\frac{1}{8\pi\mu_{\alpha\alpha}}\frac{c_1}{\Lambda^3} \tag{4.52}$$

and the function

$$f_n = \frac{n}{\Lambda^n}\int_0^\infty dq q^{n-1}\frac{8\alpha\pi\mu_{\alpha\alpha}}{q(e^{\frac{8\alpha\pi\mu_{\alpha\alpha}}{q}} - 1)}. \tag{4.53}$$

The resulting values for the various c_0 and c_1 are represented in the figures 4.8 and 4.9. As one can see, the $\alpha\alpha$ case presents an extremely strong decrease as we approach the limits below which we stay in EFT territory, while the αn

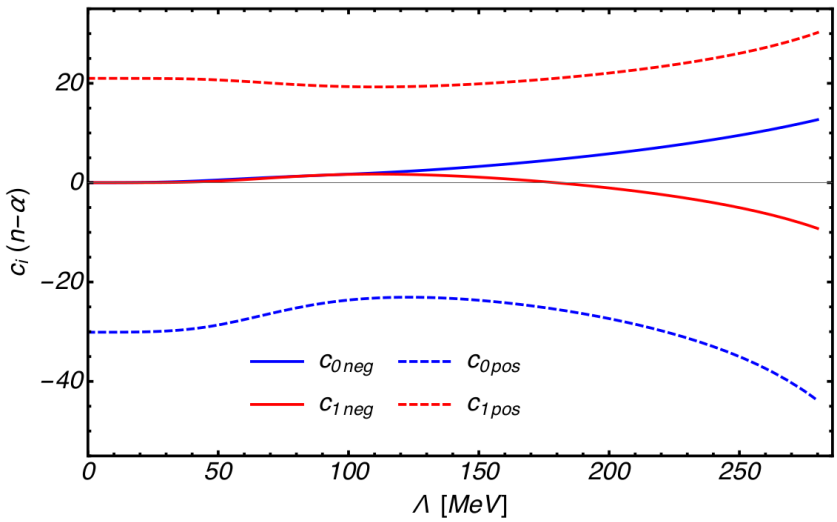

Figure 4.8: c_0 and c_1 for αn case as functions of Λ. $c_{0_{neg}}$ and $c_{1_{neg}}$ are those obtained from the solutions with the minus sign in the previous equations while $c_{0_{pos}}$ and $c_{1_{pos}}$ are those obtained with the plus sign.

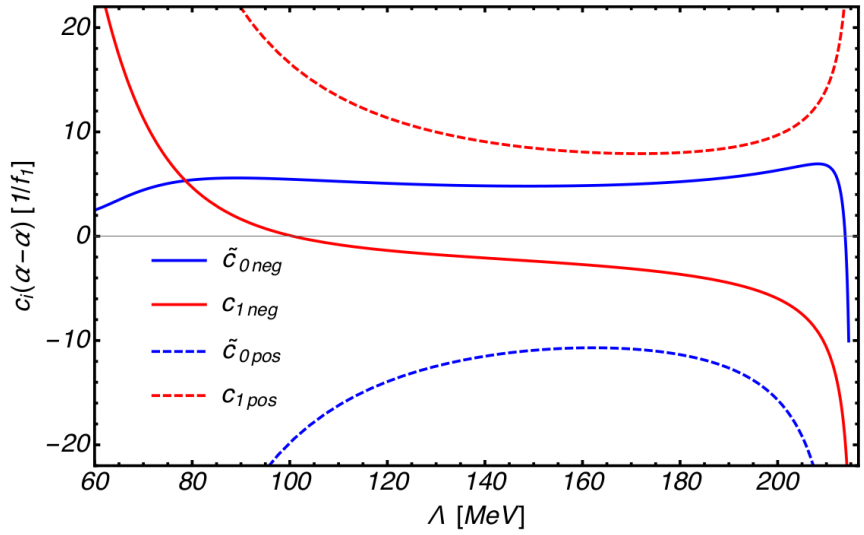

Figure 4.9: $\widetilde{c}_0$ and c_1 for $\alpha\alpha$ case as functions of Λ. $\widetilde{c}_{0_{neg}}$ and $c_{1_{neg}}$ are those obtained from the solutions with the minus sign in the previous equations while $\widetilde{c}_{0_{pos}}$ and $c_{1_{pos}}$ are those obtained with the plus sign.

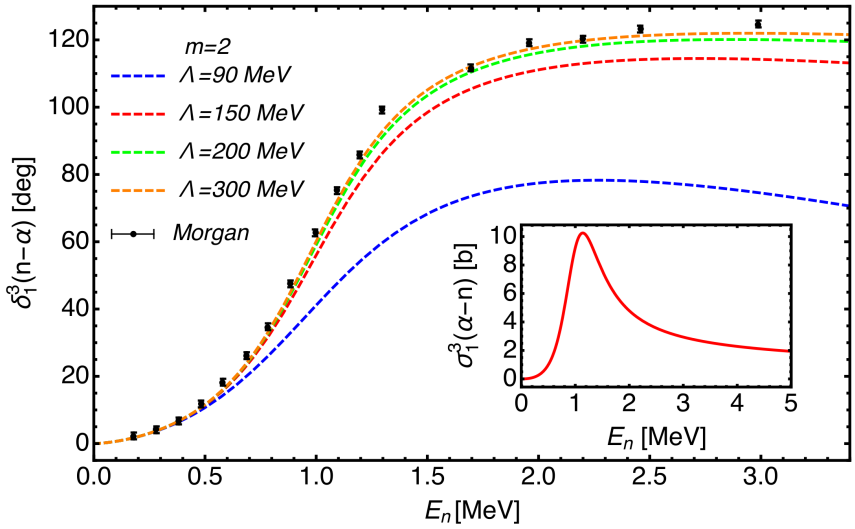

Figure 4.10: Phase shifts $\delta_3^1(E_n)$ $(l = 1, J = 3/2)$ with experimental data from Morgan and Walter [10] and in the inset the cross section $\sigma_0(E_n)$ obtained at $\Lambda = 300$ MeV.

interaction has a softer limit. These limits are given by the equations defining c_0 and c_1, where we can see that, in order to have a real value for these coefficients, one needs to limit Λ to 215 MeV for the $\alpha\alpha$ interaction and roughly 340 MeV for the αn interaction.

Also, as seen from the previous equations, there is the presence of a Wigner bound for both cases, a limit on the cutoff given by the relation with the finiteness of the effective range, these being

$$r_1 < -\frac{\Lambda}{9\pi} \tag{4.54}$$

for the αn case and

$$r_0 \to -\frac{4}{\pi\Lambda}\left[\frac{3}{f_3}\frac{1}{\left(c_1\frac{f_3}{3}-1\right)^2} - f_{-1}\right] \leq 0 \tag{4.55}$$

in the $\alpha\alpha$ case.

As one can see from figure 4.10, where the phase shifts and the cross sections calculated at various levels of Λ are shown, from a cutoff $\Lambda = 200$ MeV the phase shift is reproduced with quite an high accuracy and the the total cross section reproduces the resonance at $E_R = m_\alpha/(m_\alpha + m_n)E_{R,n} = Q_{\alpha-decay}(^5\text{He}) = 0.798$ MeV with $\Gamma_r = 0.648$ MeV.

Instead, for the $\alpha\alpha$ case, as seen in figure 4.11, where the phase shifts and cross section for this other interaction are shown, the minimum threshold for Λ is

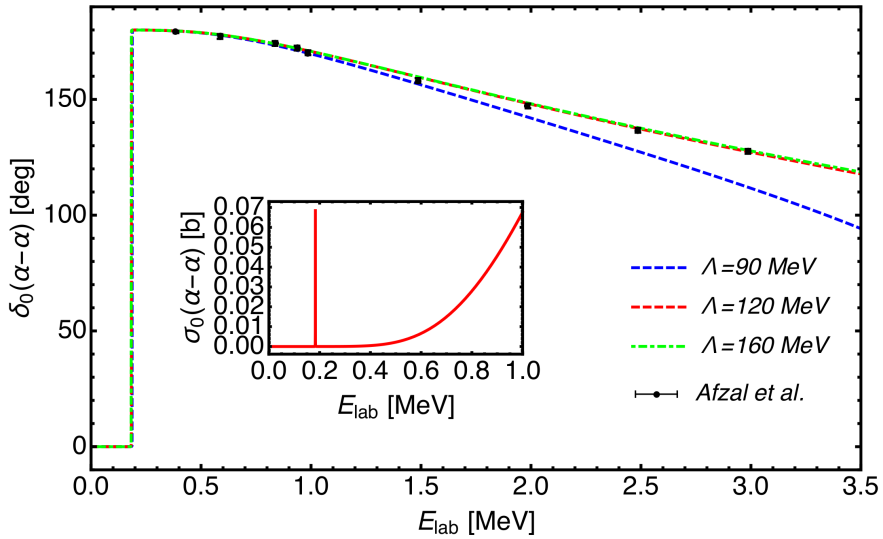

Figure 4.11: Phase shifts $\delta_0(E_{lab})$ with experimental data from Afzal et al. [11] and in the inset the cross section $\sigma_0(E_{lab})$ obtained at $\Lambda = 200$ MeV.

around 120 MeV. In this case the important resonance is ^{8}Be, that can be seen from the aforementioned figure to be at $E_R = Q_{\alpha-decay}{}^8\text{Be} = 91.8$ keV, with a width $\Gamma_R = 5.57 \pm 0.25$ eV, in agreement with the experimental data.
The last step to follow is to combine this cluster EFT potential with the program that has been developed, shown in the previous chapters, in the cases of the cluster nuclei ^{12}C and ^{9}Be.

Chapter 5

Results

Contents

5.1 The Carbon-12 nucleus

The first nucleus that was analyzed with the new potential was the Carbon-12 nucleus.
The test benchmarks on this system were already presented in the third chapter, and they showed both the accuracy of the program, being able to predict correctly the results using an Ali-Bodmer potential with a known ground state energy value, and the validity of the calculation, after transformation through Fourier transform, in momentum space.
The the final calculation of the ground state energy of Carbon-12 with the aforementioned cluster EFT potential, the result of which can be seen in figure 5.1, yields a couple of interesting results.

1. The speed of convergence: one reaches quite a good convergence already at $K = 10$, suggesting a very fast convergence for this type of potential. This can be explained by looking at the expression of this interaction: as seen in Eq. (4.30), the $\alpha\alpha$ interaction is quite simple in form (being the terms $P_l(\hat{\boldsymbol{p}} \cdot \hat{\boldsymbol{p}}')$, p^l and p'^l equal to 1 for $l = 0$), resulting in quite a soft, fast converging potential.

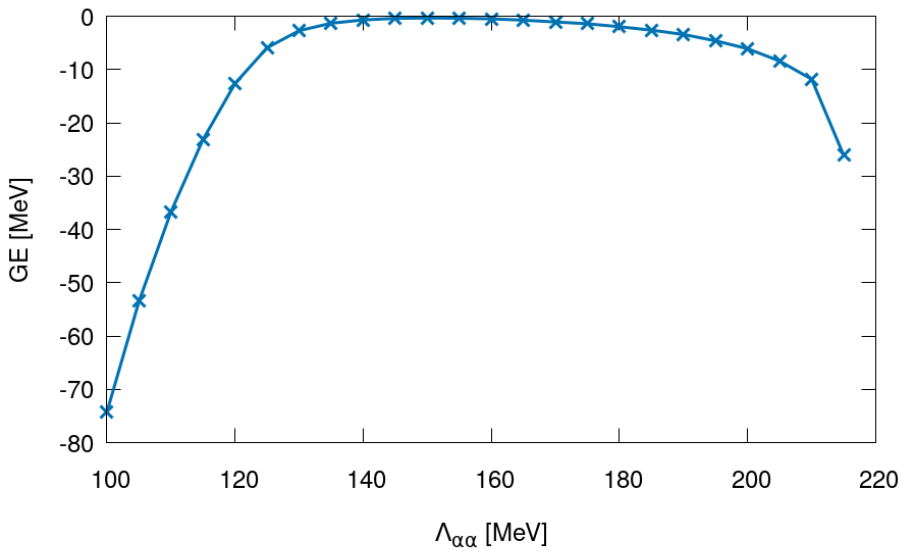

Figure 5.1: Ground state energy of ^{12}C calculated using the cluster EFT potential at different levels of the cutoff $\Lambda_{\alpha\alpha}$ shown at various levels of the hypermomentum K.

2. The range for the binding energy, with a local upper limit of -0.348 MeV at $\Lambda_{\alpha\alpha} \simeq 150$ MeV and a lower limit growing as $\Lambda_{\alpha\alpha}$ increases or decreases. The local maximum is in the expected range: at a smaller scale one has a potential that excludes too much high-momenta physics, while, at a larger scale, one is too close to the limit given by the use of an Effective Theory. The final result, in the local maximum, however is smaller than the expected binding energy of roughly 7 MeV. There are several reasons for this result: first, one can see that there is a dirscrepancy given by the inherent nature of the effective potentials: executing the cluster simplification by reducing greatly the number of interacting particles, from 12 particles (with all the 66 possible couples) to 3 (only three couples), a price has been paid. And such a price comes, in this case, in the form of three-body forces. By removing degrees of freedom in the particle number one obtains many-body forces, that are still not accounted for the final result. Second, the cutoff that has been employed. Although one starts with a theta function cutoff in the bare potential, the Coulomb dressed regulator only 'look' like a theta cutoff at a certain range. Therefore we made an approximation in that case. It might be good enough in the two body case, but the error may be enlarged in the three body case. The use

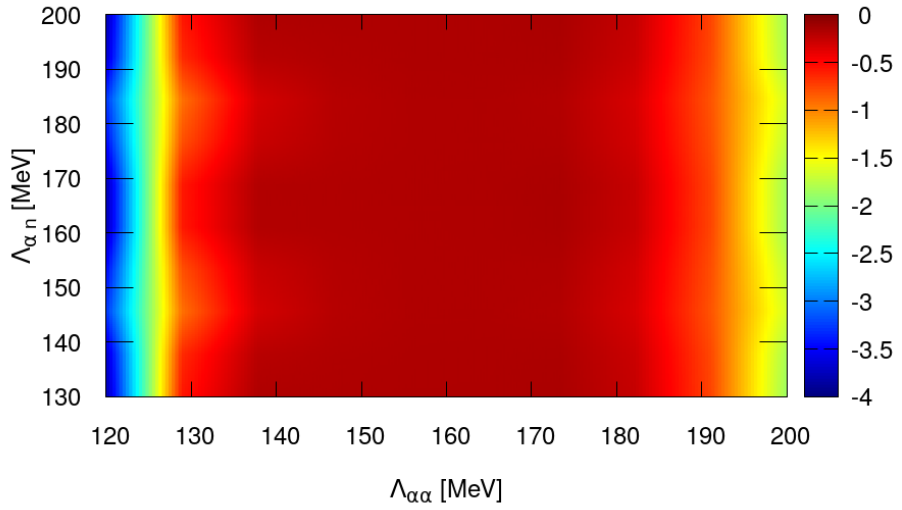

Figure 5.2: Heatmap showing the ground state energy of ^{9}Be calculated using the cluster EFT potential for different cutoffs $\Lambda_{\alpha\alpha}$ and $\Lambda_{\alpha n}$.

of a smoother regulator function therefore should be more rigorous and more accurate.

5.2 The Beryllium-9 nucleus

This program, the product of this thesis, has been then used for the calculation of the ground state energy of the Beryllium-9 nucleus through the use of the already introduced cluster EFT potential.

The results can be seen in figure 5.2. As one can see, the first thing that catches one's eye is the presence of a maximum. At a level of cutoff for $\alpha\alpha$ equal to the one for Carbon-12 and at 160 MeV for $\Lambda_{\alpha n}$, there is a maximum level for the binding energy of Beryllium-9 at 0.152 MeV. Like the case of Carbon-12 before, the binding energy is too small. However the result is much closer than before to the real value, since the total binding energy of ^{9}Be is 58.164 MeV, from which one has to remove the binding energy of both α clusters (two times 28.296 MeV, 56.164 MeV), meaning that the remaining binding energy for the cluster system is 1.572 MeV. As before, the difference between the two value is probably given by both the lack of a three-body force and the use of a step-function cutoff.

Another interesting behaviour is observed if one continues increasing or decreasing the cutoff level after reaching the maximum. As predicted, reaching a little

over 210 MeV for $\Lambda_{\alpha\alpha}$ (or a little under than 130 MeV) the ground state energy begins rapidly descending, reaching the level of more than one MeV of change in the result for a MeV of change in the cutoff. In the range considered, instead, the αn interaction has a very small dependence on the cutoff, mainly due to the bigger range allowed for its Λ.

Chapter 6

Summary and outlook

My thesis work consisted in setting up a program for the diagonalization of a nonrelativistic momentum space Hamiltonian for various particle systems. Such particles can differ between each other for mass, charge, spin and isospin. In particular it was used for calculations of cluster nuclei, Carbon-12 and Beryllium-9, using a momentum space cluster EFT potential.
After a brief chapter of introduction, where I showed the experimental and theoretical results obtained until now in the study of the Beryllium-9 photodisintegration, I've introduced the chosen basis where the calculations were made, the HH basis. Therefore in the second and third chapters it was shown a detailed description of the HH basis both in coordinate and momentum space, from the definition of the Jacobi coordinates to the calculations needed in the case of a nonlocal potential. Due to the difference between local and nonlocal potential and the difference between the two spaces it was necessary to completely restructure the original code.
At the end of the third chapter I showed several benchmark tests on different systems from tritium to Beryllium-9, passing through Helium-3 and Carbon-12, demonstrating how the new program was able to reproduce the results of the existing coordinate space program, it was also able to reproduce the results in the literature (Carbon-12 using an Ali-Bodmer potential).
The fourth chapter was an introduction to Effective Field Theory, with several examples of the application of effective theories, and I gave an overview over the history of cluster effective theory and how it was used for the Beryllium and Carbon nuclei. In the last part it was reported how to obtain the cluster EFT potential. The latter was used in the fifth chapter for the calculations of the ground state energies of Carbon-12 and Beryllium-9. Both nuclei showed a dif-

ferent energy from the experimental results at all values of cutoff. The Carbon result shows a similar underbinding to the case obtained with the Ali-Bodmer potential, while the Beryllium nucleus instead shows an overbinding.
The basis for this work was a program able to calculate the binding energy of fermions of different masses. I expanded and evolved greatly such a program by including the possibility to compute different types of particles and interactions, adding potentials that can be local and nonlocal, in coordinate space and in momentum space, between fermions and bosons.
The final product, as shown in the previous chapters, is a program able to move from simple systems like the tritium nucleus to more complex systems, up to cluster nuclei in which the constituents interact through effective field theory potentials. This opens the possibility of further calculations, with other systems and other EFT interactions.
In future, the first point to explore is the substitution of the step function cutoff in the $\alpha\alpha$ potential by a Gaussian one, similarly to the case of αn. While the calculation for the λ_0 and λ_1 coefficients in Eq. (4.24) becomes considerably more difficult, the change from such a sharp cutoff to a softer should improve the results of the calculations, for the reasons stated in the previous chapter. The calculations withthis new regulator are only in the first stages, but the first results seem to be promising.
However, this is not the only possible development that can be made with this program. The missing three-body force generated by the EFT approach is another problem that need to be tackled. Looking back at the chapter about the hyperspherical basis one can then see that the future implementation of three-body interactions in the program is a feasible idea: adding to the hyperradius and last hyperangle, as a variable of integration, the second-to-last hyperangle one can then use interactions that take into account the third particle in addition to the first two. Adding permutation matrices the three-body force can be extended to all the possible triplets of the system, allowing the use of better EFT potentials.
Another possible future project is the study of ^{9}Be photodisintegration.
As it was stated in the Introduction, the photodisintegration of ^{9}Be is an interesting reaction because it is the inverse process of $\alpha + \alpha + n \rightarrow ^9\text{Be}+\gamma$, the first step in Carbon-12 production through the $\alpha\alpha n$ chain, which is hypothesized to be the main path of carbon generation in supernovae. In order to study this process one needs to calculate the photoabsorption cross-section, which can be expressed in terms of the response function $r(E)$.
The idea is then to employ the so-called Lorentz Integral Transform (LIT) tech-

nique [39], that transforms the continuum problem to a bound state like problem. In the case of an inclusive reaction, as for example the total photodisintegration cross section of a nucleus, one needs to determine a response function $r(E)$ of the following type

$$r(E) = \sum\!\!\!\!\!\!\int_{\gamma} \langle\psi_0|\,\hat{O}^\dagger\,|\psi_\gamma\rangle\,\langle\psi_\gamma|\,\hat{O}\,|\psi_0\rangle\,\delta(E_\gamma - E), \tag{6.1}$$

where ψ_0 is the nuclear ground state wave function and ψ_γ the wave function of an excited state of the nucleus, and $\hat{O}$ is an operator that induces the transition. The LIT is defined as follows

$$L(\sigma_R, \sigma_I) = \sum\!\!\!\!\!\!\int K(\sigma, E) r(R) dE = \left\langle \widetilde{\psi} \middle| \widetilde{\psi} \right\rangle, \tag{6.2}$$

with the Lorentzian kernel $K(\sigma, E)$ defined as

$$K(\sigma, E) = \frac{1}{(E - E_0 + \sigma_R)^2 + \sigma_I}, \tag{6.3}$$

and $\sigma = E_0 + \sigma_R + \sigma_I$, E_0 being the ground state energy.
The LIT state is obtained from

$$(\hat{H} - E_0 - \sigma_R - i\sigma_I) \left|\widetilde{\psi}\right\rangle = \hat{O}\,|\psi_0\rangle\,. \tag{6.4}$$

After having determined the LIT one needs to invert the transform in order to determine $r(E)$.
The equation (6.4) can be solved with bound state methods, the solution is based on the diagonalization of the Hamiltonian for a given final channel. For this part of the solution the program developed in this thesis can be used.
For the low-energy ^{9}Be photodisintegration one can use the electric dipole operator $\hat{D}$ as $\hat{O}$ hence the possible final channels must satisfy

$$\begin{cases} \Delta l = 0, \pm 1 \\ \Delta s = 0. \\ \pi_f = -\pi_i \end{cases} \tag{6.5}$$

Since ^{9}Be ground state is $J^\pi = 3/2^-$, one finds three possible final channels: $1/2^+$, $3/2^+$ and $5/2^+$.
The program isn't limited to deal only with cluster nuclei, it is also possible to study nucleonic systems interacting through chiral EFT (χEFT) potentials.

Bibliography

[1] C. W. Arnold, T. B. Clegg, C. Iliadis, H. J. Karwowski, G. C. Rich, J. R. Tompkins, and C. R. Howell, "Cross-section measurement of ^{9}Be(γ,n)^{8}Be and implications for $\alpha+\alpha+n \rightarrow^{9}$Be in the r process," *Phys. Rev. C*, vol. 85, p. 044605, Apr 2012.

[2] Burda, O. and von Neumann-Cosel, P. and Richter, A. and Forssen, C. and Brown, B. A., "Resonance parameters of the first 1/2+ state in ^{9}Be and astrophysical implications," *Phys. Rev.*, vol. C82, p. 015808, 2010.

[3] H. Utsunomiya, Y. Yonezawa, H. Akimune, T. Yamagata, M. Ohta, M. Fujishiro, H. Toyokawa, and H. Ohgaki, "Photodisintegration of ^{9}Be with laser-induced Compton backscattered γ rays," *Physical Review C*, vol. 63, May 2000.

[4] J. H. Gibbons, R. L. Macklin, J. B. Marion, and H. W. Schmitt, "Precision Measurement of the ^{9}Beγ, n) Cross Section," *Phys. Rev.*, vol. 114, pp. 1319–1323, Jun 1959.

[5] R. Hughes, R. Sambell, E. Muirhead, and B. Spicer, "The photoneutron cross section of ^{9}Be," *Nuclear Physics A*, vol. 238, no. 2, pp. 189 – 198, 1975.

[6] M. Fujishiro, T. Tabata, K. Okamoto, and T. Tsujimoto, "Cross section of the reaction ^{9}Be(γ, n) near threshold," *Canadian Journal of Physics*, vol. 60, no. 11, pp. 1672–1677, 1982.

[7] P. Lepage, "How to Renormalize the Schrodinger Equation," *arXiv e-prints*, pp. nucl–th/9706029, Jun 1997.

[8] L. R. Hafstad and E. Teller, "The Alpha-Particle Model of the Nucleus," *Phys. Rev.*, vol. 54, pp. 681–692, Nov 1938.

[9] T. Kokalova Wheldon, "Over half a century of studying Carbon-12," *Journal of Physics: Conference Series*, vol. 639, 09 2015.

[10] G. L. Morgan and R. L. Walter, "Neutron-Helium Interaction. II. Angular Distributions and Phase Shifts from 0.2 to 7.0 MeV," *Phys. Rev.*, vol. 168, pp. 1114–1130, Apr 1968.

[11] S. Afzal, A. Ahmad, and S. Ali, "Systematic Survey of the α-α Interaction," *Rev. Mod. Phys.*, vol. 41, pp. 247–273, Jan 1969.

[12] E. M. Burbidge, G. R. Burbidge, W. A. Fowler, and F. Hoyle, "Synthesis of the Elements in Stars," *Rev. Mod. Phys.*, vol. 29, pp. 547–650, Oct 1957.

[13] M. Froissart, "Asymptotic Behavior and Subtractions in the Mandelstam Representation," *Phys. Rev.*, vol. 123, pp. 1053–1057, Aug 1961.

[14] U. Kneissl, G. Kuhl, K.-H. Leister, and A. Weller, "Photoneutron cross sections for 9Be obtained with quasi-monoenerget1c photons," *Nuclear Physics A*, vol. 247, no. 1, pp. 91 – 102, 1975.

[15] B. Russell, D. Sachs, A. Wattenberg, and R. Fields, "Yields of Neutrons from Photo-Neutron Sources," *Phys. Rev.*, vol. 73, pp. 545–549, Mar 1948.

[16] B. Hamermesh and C. Kimball, "The Photodisintegration Cross Section of Beryllium at 2.185 Mev," *Physical Review*, vol. 90, no. 6, p. 1063–1065, 1953.

[17] V.D. Efros and H. Oberhummer and A. Pushkin and I.J. Thompson, "Low-energy photodisintegration of ^{9}Be and $\alpha + \alpha + n \leftrightarrow ^9$Be $+\gamma$ reactions at astrophysical conditions," *Eur. Phys. J. A*, vol. 1, no. 4, pp. 447–453, 1998.

[18] J. Casal, M. Rodríguez-Gallardo, J. M. Arias, and I. J. Thompson, "Astrophysical reaction rate for ^{9}Be formation within a three-body approach," *Phys. Rev. C*, vol. 90, p. 044304, Oct 2014.

[19] N. Barnea, *Exact solution of the Schrödinger and Faddeev equations for few body systems*. PhD thesis, Hebrew University, 1997.

[20] N. Y. Vilenkin, G. I. Kuznetsov, and Y. A. Smorodinskii, "Eigenfunctions of the Laplace Operator Providing Representations of U(2),SO(3),U(3) and SU(3) Groups and the Symbolic Method," *Sov. J. Nucl. Phys.*, pp. 906–917, November 1965.

[21] N. Barnea, W. Leidemann, and G. Orlandini, "Ground state wave functions in the hyperspherical formalism for nuclei with A greater than 4," *Nucl. Phys.*, vol. A650, pp. 427–442, 1999.

[22] M. Gattobigio, A. Kievsky, and M. Viviani, "Nonsymmetrized hyperspherical harmonic basis for an A-body system," *Phys. Rev. C*, vol. 83, p. 024001, Feb 2011.

[23] F. F. Ruffino, *Non-Symmetrized Hyperspherical Harmonics Method Applied to Light Hypernuclei.* PhD thesis, University of Trento, 2017.

[24] J. Raynal and J. Revai, "Transformation coefficients in the hyperspherical approach to the three-body problem," *Il Nuovo Cimento A (1965-1970)*, vol. 68, pp. 612–622, Aug 1970.

[25] M. Viviani, L. E. Marcucci, S. Rosati, A. Kievsky, and L. Girlanda, "Variational Calculation on A = 3 and 4 Nuclei with Non-Local Potentials," *Few-Body Systems*, vol. 39, pp. 159–176, Sep 2006.

[26] V. D. Efros, "Elimination of Rotational Degrees of Freedom in Expansion Methods for Three Nucleons," *Few-Body Systems*, vol. 32, pp. 169–181, Oct 2002.

[27] D. Thompson, M. Lemere, and Y. Tang, "Systematic investigation of scattering problems with the resonating-group method," *Nuclear Physics A*, vol. 286, no. 1, pp. 53 – 66, 1977.

[28] R. Malfliet and J. Tjon, "Solution of the Faddeev equations for the triton problem using local two-particle interactions," *Nuclear Physics A*, vol. 127, no. 1, pp. 161 – 168, 1969.

[29] E. M. Tursunov, D. Baye, and P. Descouvemont, "Comparative variational studies of 0+ states in three-α models," *Nuclear Physics A*, vol. 723, pp. 365–374, 08 2003.

[30] C. Manzata, "Ground State and Photodisintegration of Beryllium-9 in Cluster Effective Field Theory," Master's thesis, University of Trento, 2016.

[31] Sudarshan,E. C. G. and Marshak,R. E. , "Origin of the Universal V-A theory," *AIP Conference Proceedings*, vol. 300, no. 1, pp. 110–124, 1994.

[32] R. B. Wiringa, S. C. Pieper, J. Carlson, and V. R. Pandharipande, "Quantum Monte Carlo calculations of $A = 8$ nuclei," *Phys. Rev. C*, vol. 62, p. 014001, Jun 2000.

[33] D. Brink and J. Castro, "Alpha clustering effects in nuclear matter," *Nuclear Physics A*, vol. 216, no. 1, p. 109–124, 1973.

[34] H. Horiuchi and K. Ikeda, "A Molecule-like Structure in Atomic Nuclei of 16O* and 10Ne," *Progress of Theoretical Physics*, vol. 40, no. 2, pp. 277–287, 1968.

[35] F. Hoyle, "On Nuclear Reactions Occuring in Very Hot STARS.I. the Synthesis of Elements from Carbon to Nickel.," *Astrophysical Journal, Supplement*, vol. 1, p. 121, Sep 1954.

[36] Cook, C. W. and Fowler, W. A. and Lauritsen, C. C. and Lauritsen, T., "^{12}B, ^{12}C, and the Red Giants," *Phys. Rev.*, vol. 107, pp. 508–515, Jul 1957.

[37] M. Freer, "The clustered nucleus—cluster structures in stable and unstable nuclei," *Reports on Progress in Physics*, vol. 70, no. 12, p. 2149, 2007.

[38] C. Ji, C. Elster, and D. R. Phillips, "^{6}He nucleus in halo effective field theory," *Phys. Rev. C*, vol. 90, p. 044004, Oct 2014.

[39] V. D. Efros, W. Leidemann, G. Orlandini, and N. Barnea, "The Lorentz integral transform (LIT) method and its applications to perturbation-induced reactions," *Journal of Physics G: Nuclear and Particle Physics*, vol. 34, pp. R459–R528, oct 2007.